The Astrophysical Journal, 788:109 (19pp), 2014 June 20 doi:10.1088/0004-637X/788/2/109

PROBABILITY FRIENDS-OF-FRIENDS (PFOF) GROUP FINDER: PERFORMANCE STUDY AND OBSERVATIONAL DATA APPLICATIONS ON PHOTOMETRIC SURVEYS

Hung-Yu Jian[1], Lihwai Lin[2], Tzihong Chiueh[1,3,4], Kai-Yang Lin[2], Hauyu Baobab Liu[2], Alex Merson[5,6], Carlton Baugh[6], Jia-Sheng Huang[7,8], Chin-Wei Chen[2], Sebastien Foucaud[2,9], David N. A. Murphy[10], Shaun Cole[6], William Burgett[11], and Nick Kaiser[11]
[1] Department of Physics, National Taiwan University, 106, Taipei, Taiwan, Republic of China; hyj@phys.ntu.edu.tw
[2] Institute of Astronomy & Astrophysics, Academia Sinica, 106, Taipei, Taiwan, Republic of China
[3] Center for Theoretical Sciences, National Taiwan University, 106, Taipei, Taiwan, Republic of China
[4] LeCosPa, National Taiwan University, 106, Taipei, Taiwan, Republic of China
[5] Department of Physics and Astronomy, University College London, Gower Street, London WC1E 6BT, UK
[6] Institute for Computational Cosmology, Department of Physics, Durham University, South Road, Durham DH1 3LE, UK
[7] National Astronomical Observatories, Chinese Academy of Sciences, Beijing 100012, China
[8] Harvard-Smithsonian Center for Astrophysics, 60 Garden Street, Cambridge, MA 02138, USA
[9] Department of Earth Sciences, National Taiwan Normal University, N.88, Tingzhou Road, Sec. 4, Taipei 11677, Taiwan, Republic of China
[10] Department of Astronomy and Astrophysics, Pontificia Universidad Católica de Chile, Vicuña Mackenna 4860, 7820436 Macul, Santiago, Chile
[11] Institute for Astronomy, University of Hawaii, 2680 Woodlawn Drive, Honolulu, HI 96822, USA
Received 2013 May 7; accepted 2014 April 29; published 2014 May 28

ABSTRACT

In tandem with observational data sets, we utilize realistic mock catalogs, based on a semi-analytic galaxy formation model, constructed specifically for Pan-STARRS1 Medium Deep Surveys to assess the performance of the Probability Friends-of-Friends (PFOF) group finder, and aim to develop a grouping optimization method applicable to surveys like Pan-STARRS1. Producing mock PFOF group catalogs under a variety of photometric redshift accuracies ($\sigma_{\Delta z/(1+z_s)}$), we find that catalog purities and completenesses from "good" ($\sigma_{\Delta z/(1+z_s)} \sim 0.01$) to "poor" ($\sigma_{\Delta z/(1+z_s)} \sim 0.07$) photo-$z$s gradually degrade from 77% and 70% to 52% and 47%, respectively. A "subset optimization" approach is developed by using spectroscopic-redshift group data from the target field to train the group finder for application to that field and demonstrated using zCOSMOS groups for PFOF searches within PS1 Medium Deep Field04 (PS1MD04) and DEEP2 EGS groups in PS1MD07. With four data sets spanning the photo-z accuracy range from 0.01 to 0.06, we find purities and completenesses agree with their mock analogs. Further tests are performed via matches to X-ray clusters. We find PFOF groups match ∼85% of X-ray clusters identified in COSMOS and PS1MD04, lending additional support to the reliability of the detection algorithm. In the end, we demonstrate, by separating red and blue group galaxies in the EGS and PS1MD07 group catalogs, that the algorithm is not biased with respect to specifically recovering galaxies by color. The analyses suggest the PFOF algorithm shows great promise as a reliable group finder for photometric galaxy surveys of varying depth and coverage.

Key words: galaxies: clusters: general – galaxies: groups: general – large-scale structure of universe – methods: data analysis

Online-only material: color figures

1. INTRODUCTION

In the Λ cold dark matter (ΛCDM) cosmology, structures grow hierarchically, with small objects forming initially from very small density fluctuations and merging successively to become the large-scale structures we detect today (Peebles 1982; Blumenthal et al. 1984; Davis et al. 1985; Springel et al. 2005). The study of the formation and evolution of large-scale structures is, therefore, important for improving our understanding of the universe on both cosmological and galactic scales. As the largest bound objects in the universe, clusters of galaxies are naturally the structures appropriate for such a study. The high mass end of the mass distribution of collapsed structures, i.e., galaxy clusters and groups, is the most accessible observationally and hence cluster masses often serve as probes to constrain the cosmological parameters (e.g., Carlberg et al. 1996; Borgani et al. 2001; Schuecker et al. 2003; Mantz et al. 2008; Allen et al. 2011). Additionally, galaxy clusters are also ideal sites for gravitational lensing studies of the dark matter (e.g., Sheldon et al. 2004; Wittman et al. 2006; Smail et al. 2007) due to the dominance of dark matter over baryons, contributing ∼85% of the whole mass content. Clusters not only have strong X-ray signatures due to the hot intracluster gas trapped inside deep gravitational potentials (Sarazin 1986), but the hot gas also leaves an imprint on the cosmic microwave background through the Sunyaev–Zel'dovich effect (Sunyaev & Zel'dovich 1980; Carlstrom et al. 2002; Lin et al. 2004). Many studies indicate that clusters are important laboratories for investigating galaxy evolution (e.g., Oemler 1974; Lin et al. 2004; Voit 2005).

Moreover, some studies have suggested the presence of a critical halo mass, roughly corresponding to the mass of the group scale, above which star formation is efficiently quenched (e.g., Dekel & Birnboim 2006; Gilbank & Balogh 2008). The group environment is also an important location for studying galaxy formation and evolution. Observationally, it has been found that the galaxy merger rate depends strongly on environment (Lin et al. 2010; de Ravel et al. 2011; Kampczyk et al. 2013), and evidence from semi-analytical models implemented in the Millennium Simulation shows that galaxies in denser environments tend to have higher merger rates than those in the fields; these higher density regions are primarily dominated by group environments (Jian et al. 2012). It is therefore of great importance to

produce reliable catalogs of galaxy groups and clusters that can be used to study the role of environment in galaxy evolution.

In the optical regime, group identification has been attempted over a number of years. Methods for group finding in galaxy surveys can be roughly divided into two categories: methods using spectroscopic data and those using photometric data. Spectroscopic galaxy redshift surveys can reduce much of the projection effect problem except for the fingers-of-God effect due to galaxy motion inside virialized structures. The Friends-of-friends (FOF) algorithm (Huchra & Geller 1982) is one of the most popular approaches to group finding and is still in common use in present-day redshift surveys (Knobel et al. 2009, 2012). FOF plus simple assumptions about the properties of galaxies in groups and clusters is also in use (e.g., Eke et al. 2004; Yang et al. 2005). In addition, the Voronoi–Delaunay Method (VDM) of Marinoni et al. (2002), which is claimed to compensate for some of the shortcomings of the traditional FOF algorithm, is also a common method used for group identification. This latter method was adopted by the DEEP2 collaboration (Gerke et al. 2005, 2012). The sparse sampling of galaxies in spectroscopic surveys is one known shortcoming of group-finding, and is a major concern for high redshift surveys, which are observationally expensive.

By contrast, photometric surveys have a much more complete sampling rate, but the foreground and background contamination can be significant, especially for modern deep photometric surveys. Therefore, group finding algorithms for this type of survey typically must include additional components to alleviate such contaminations. For example, algorithms can rely on assumptions about the properties of galaxies in clusters, such as the matched-filter or red-sequence methods (e.g., Postman et al. 1996; Gladders & Yee 2000; Koester et al. 2007; Murphy et al. 2012). Algorithms can take into account photometric redshift estimates (e.g., Li & Yee 2008; Gillis & Hudson 2011; Wen et al. 2009), including the Probability Friends-of-Friends (PFOF) algorithm (Liu et al. 2008).[12] Algorithms can also be based on a combination of the two (e.g., Milkeraitis et al. 2010). Red-sequence methods (Gladders & Yee 2000; Koester et al. 2007; Murphy et al. 2012) utilize the presence of the red-sequence ridgeline, and have been demonstrated to be successful at detecting clusters. However, their advantages can also turn into drawbacks. The identification of structures tends to be biased toward rich clusters with red galaxies. In addition, at high redshift, the presence of the red-sequence ridgeline is less clear, making the performance of red-sequence methods more uncertain. Compared to red-sequence methods, PFOF only needs information regarding the location of galaxies and photometric redshift estimates without preferential color selection, and can on one hand include blue members that are missed by red-sequence methods, while on the other hand identify groups of low richness with no red-sequence galaxies. Therefore, PFOF has its own unique advantages.

In the past few decades, large area, deep optical and infrared galaxy surveys have shown rich group and cluster structures on various scales. Nowadays, surveys of even greater area and deeper multiband optical sky surveys, such as Pan-STARRS (Kaiser et al. 2002) or the Dark Energy Survey (Frieman et al. 2013), have been carried out to image more of the universe. Forthcoming surveys such as those with the Subaru Hyper Suprime-Cam (Takada 2010) or the Large Synoptic Survey Telescope (Ivezic et al. 2008) will also start soon. With such a huge amount of data, a reliable group finder is obviously needed for group and cluster studies. We shall show in this paper that PFOF is a highly competitive tool for this purpose.

This work is the extension of Liu et al. (2008, hereafter Liu08). In Liu08, the algorithm, PFOF, was presented and simple tests based on DEEP2 mock catalogs were carried out. In this paper, we extend Liu08 by adding further tests of the performance of PFOF. We adopt an improved Durham Pan-STARRS1 mock catalog, which has a larger field of view and greater depth, for use in various tests to demonstrate the performance of PFOF. In additional to scaling the linking length to the mean separation of galaxies as a function of redshift, we also adopt an optimization measure introduced by Knobel et al. (2012) to produce the optimal catalogs. Moreover, we apply "subset optimization" which utilizes spectral-z groups as a training set, to the observational data to optimize the PFOF group catalog, so as to avoid any model dependency through using the mock catalog. Data sets with "good" photometric redshift accuracy, $\sigma_{\Delta z/(1+z_s)} \sim 0.01$ in COSMOS, "medium" accuracy $\sigma_{\Delta z/(1+z_s)} \sim 0.03$ in EGS, and relatively "poor" accuracy $\sigma_{\Delta z/(1+z_s)} \sim 0.06$ in Pan-STARRS1 Medium-Deep04 (PS1MD04) and PS1MD07 are tested to understand the dependence of the optimal performance on photo-z accuracy and to evaluate the applicability of PFOF. Finally, results are also compared with a X-ray catalogs to demonstrate the success of the subset optimization and the PFOF capability.

This paper represents the first in a series of studies using PS1 medium deep surveys (MDS) based on the version of data reduction provided by S. Foucaud et al. (2013, in preparation). In Lin et al. (2014), the environmental effect on the star formation rate in PS1 MDS data will be studied. This paper is structured as follows. In Section 2, we briefly describe the data sets we use, including the Durham mock, one X-ray, two spectral-z catalogs, and four photometric-redshift galaxy catalogs. The PFOF algorithm as well as definitions of purity and completeness are then introduced in Section 3. Tests of the mock data for PFOF are illustrated in Section 4. In Section 5, observational data applications and performance tests for PFOF are provided. Finally, we give our summary and discussion in Section 6. Throughout this paper, we adopt the following cosmology: $H_0 = 100\ h\,\mathrm{km\,s^{-1}\,Mpc^{-1}}$, where the Hubble constant $h = 0.73$, matter density $\Omega_m = 0.24$, and cosmological constant $\Omega_\Lambda = 0.76$.

2. DATA

2.1. Mock Pan-STARRS Medium Deep Survey Catalog

The mock catalog that we use to evaluate the performance of our group finder is based on the Millennium dark matter N-body simulation (Springel et al. 2005). Halos in the simulation are first identified using an FOF halo finder (Davis et al. 1985) with a linking length of $b = 0.2$ in units of the mean particle separation. Each FOF-identified halo is then broken into constituent subhalos by the SUBFIND algorithm (Springel et al. 2001), which identifies gravitationally bound substructures within the host FOF halo. With all halos and subhalos determined, the hierarchical merging trees containing the details of how structures build up over cosmic time can then be constructed. These trees are the key information needed to compute the physical properties of the associated galaxy population for semi-analytical models. The mock catalog adopts the Lagos et al. (2012) model

[12] Li & Yee (2008) also developed a group searching method in photometric-redshift space with the identical name, the probability Friends-of-Friends algorithm, to ours. However, two grouping methods have distinct algorithms and selection functions. We stress here that the reader should be cautious not to become confused by the name.

which takes advantage of the extension to the treatment of star formation introduced into GALFORM (Cole et al. 2000) in Lagos et al. (2011) to populate galaxies, and is then assembled into a lightcone (Merson et al. 2013). The data set covers an area of 50.25 deg^2 and includes PS1 $g_{\rm P1}r_{\rm P1}i_{\rm P1}z_{\rm P1}y_{\rm P1}$ photometry for galaxies down to a magnitude limit of $i_{\rm P1} < 25.8$ and a redshift range up to $z \sim 3$. A central area of $\sim$7 deg^2 has been selected for our analyses, which is equivalent to a single pointing of PS1, the area of a single MDS tile. This mock field contains 1,601,486 galaxies with $i_{\rm P1} < 25.8$ and 7,756 groups, i.e., the halos in the simulation, with richness $N \geqslant 4$.

The semi-analytic models are tuned to match a selection of observations of local galaxies, e.g., the field galaxy luminosity function, but are not explicitly tuned to match any group data. It is plausible that two models that match the field luminosity function could have different group properties, and may therefore suggest different parameters for the group finder. In this paper, the mock catalog is thus used only to explore the tendency of the grouping performance of PFOF under various photo-z accuracies. For real data application, we will not use the parameters obtained from the mocks.

2.2. The COSMOS Survey

In the 2-deg^2 COSMOS field (Scoville et al. 2007), the galaxy catalog adopted in our analysis is from the X-ray group membership galaxy catalog[13] described in George et al. (2011). The photo-z estimation uses an updated version (`pdzBay_v1.7_010809`) presented in Ilbert at al. (2009) with additional deep H-band data and small improvements in the template-fitting techniques. The precise redshifts in the catalog are computed with 30 broad, intermediate, and narrow bands covering the UV (*Galaxy Evolution Explorer*), visible near-IR (NIR; Subaru, Canada–France–Hawaii Telescope (CFHT), United Kingdom Infrared Telescope, and National Optical Astronomy Observatory), and mid-IR (*Spitzer*/IRAC). A redshift dispersion of $\sigma_{\Delta z/(1+z_s)}$ is $\sim$0.007 at $i^+_{AB} < 22.5$, and at fainter magnitudes $i^+_{AB} < 24$ and $z < 1.25$, the accuracy $\sigma_{\Delta z/(1+z_s)}$ is $\sim$0.012 (Ilbert at al. 2009). The catalog contains 115,844 galaxies with $i \leqslant 24.2$ and 129 X-ray groups with `FLAG_INCLUDE` = 1, indicating that these groups have high X-ray quality, more than three members, no mask, and no merger signature (George et al. 2011), and is adopted in this paper for performance assessment of surveys with "good" photo-z accuracy.

2.3. The zCOSMOS Survey and Group Catalog

zCOSMOS (Lilly et al. 2007) is a spectroscopic redshift survey covering the 1.7-deg^2 of the COSMOS field, and consists of two parts, "zCOSMOS-bright," a pure magnitude selected survey with $15 \leqslant I_{AB} \leqslant 22.5$, and "zCOSMOS-deep," aiming at observing about 10,000 galaxies in the redshift range $1.5 < z < 3.0$ selected through a well defined color criteria. zCOSMOS-bright, which covers mainly the redshift range $0.1 < z < 1.2$, almost the entire COSMOS field, is complete and contains spectra of about 20,000 objects taken using the VIMOS spectrograph with a medium-resolution grism. Knobel et al. (2009) construct an optical group catalog (the 10 k catalog) between $0.1 < z < 1$ based on $\sim$8,417 high-quality spectroscopic redshifts in the zCOSMOS-bright survey. Knobel et al. (2012) recently released an updated optical group catalog (the 20 k catalog) covering $0.1 \leqslant z \leqslant 1$, based on 16,500 high-quality spectroscopic redshifts in the completed zCOSMOS-bright survey. However, the 20 k catalog includes only group galaxies without field galaxies so that it cannot be adopted for training purposes. We thus make use of this 10 k group catalog as the training set to optimize our linking lengths and threshold for data sets covering the COSMOS field. The catalog contains 802 groups with richness $N \geqslant 2$.

[13] The catalog can be downloaded via the link: http://irsa.ipac.caltech.edu/data/COSMOS/tables/groups/.

2.4. The EGS Photometric Redshift Catalog

The EGS photometric redshift catalog has a field-of-view of 0.5-deg^2 and is based on the photometric observations in the extended Groth strip (EGS) consisting of 18 bands from u to 8 μm (Huang et al. 2013). After combining redundant bands, there are 12 wavelengths available for the photometric redshift estimation. The photo-z accuracy for this catalog is on the order of $\sim$0.025 with 3.5% outliers. The catalog contains 11,229 galaxies, and is used as for the performance test with "medium" photo-z accuracy.

2.5. The DEEP2 Survey and Group Catalog

The DEEP2 Galaxy Redshift Survey (Davis et al. 2003; Newman et al. 2013) is a spectroscopic survey covering a combined area of four separate fields of approximately 3-deg^2 down to a limiting magnitude of $R_{AB} < 24.1$, and probes a volume of $5.6 \times 10^6\ h^3$ Mpc^{-3} over the primary DEEP2 redshift range $0.75 < z < 1.4$. There are 50,000 spectra obtained in 1 hr exposures with the DEIMOS spectrograph (Faber et al. 2003) on the Keck II telescope, and in this data set 35,000 objects are confirmed with galaxy redshifts. Overall, the sampling rate is roughly 70% of the median sampling rate in the most crowded regions, and the redshift success rate is also about 70% (Newman et al. 2013).

Gerke et al. (2012) present a public catalog of galaxy groups constructed from the spectroscopic sample of galaxies using VDM in the fourth data release of the DEEP2 Galaxy Redshift Survey, including EGS. In the EGS field, the catalog contains 12,346 galaxies in the redshift range z = 0 to 1.4 down to $R_{AB} \leqslant 24.1$ and 1,165 groups with a richness of $N \geqslant 2$. The EGS field overlaps with the Pan-STARRS 1 Medium Deep Field 07 (PS1MD07) and is used as a training set for the optimization of PFOF.

2.6. The Pan-STARRS1 Medium Deep Survey

Pan-STARRS1 (Kaiser et al. 2002, 2010; Chambers 2006, 2011) is a 1.8 m optical telescope with a 7 square degree field of view that can image the sky in $g_{\rm P1}$, $r_{\rm P1}$, $i_{\rm P1}$, $z_{\rm P1}$, and $y_{\rm P1}$ filters which cover the 4000 Å $< \lambda <$ 10500 Å spectral range (Stubbs et al. 2010; Tonry et al. 2012). Images obtained by the Pan-STARRS1 system are processed through the Image Processing Pipeline (IPP; Magnier 2006). Photometric and astrometric measurements performed by the IPP system are described in Magnier (2007), Magnier et al. (2008), and Magnier et al. (2013). Photometric calibration of the Pan-STARRS1 survey is discussed in Schlafly et al. (2012).

The official deep stacks for the Medium Deep fields from IPP were not available for use. We instead adopt Foucaud's deep stacks (S. Foucaud et al. 2013, in preparation), which include the $g_{\rm P1}r_{\rm P1}i_{\rm P1}z_{\rm P1}y_{\rm P1}$ bands for all nightly stacks from 2010 April to 2011 December, plus the CFHT u-band from archival data. Astrometric and photometric calibration are performed with

Table 1
Data Sets

Catalog Name	Catalog Type	Area (deg^2)	Redshift	Flux Limit	$\sigma_{\Delta z/(1+z_s)}$	Purpose	Ref
Durham Mock	Mock	~7	$z < 3.0$	$i \leqslant 25.8$	Performance	(1)	
COSMOS	Photometric	~2	$0 < z < 1.25$	$i^+_{AB} \leqslant 24.2$	~ 0.0125 ($i^+_{AB} \leqslant 24$)	Input	(2)
EGS	Photometric	<0.5	$0 < z < 1.4$	$i \leqslant 24.1$	~0.025 to ($R \leqslant 24.1$)	Input	(3)
PS1MD04	Photometric	~7	$0 < z < 1.4$	$i_{P1} \leqslant 24.1$	~0.46 ($i_{P1} \leqslant 22.5$)	Input	(4)
PS1MD07	Photometric	~7	$0 < z < 1.4$	$i_{P1} \leqslant 24.1$	~0.51 ($i_{P1} \leqslant 24.1$)	Input	(4)
zCOSMOS	Spectroscopic	~1.7	$0 < z < 1.2$	$i_{AB} \leqslant 22.5$		Training	(5)
DEEP2 EGS	Spectroscopic	~0.5	$0 < z < 1.4$	$R_{AB} \leqslant 24.1$		Training	(6)
XMM-NEWTON+Chandra	X-ray	~2	$0 < z < 1.0$			Performance	(2)

References. (1) Merson et al. (2013); (2) George et al. (2011); (3) Huang et al. (2013); (4) S. Foucaud et al. (2013, in preparation); (5) Knobel et al. (2009); (6) Gerke et al. (2012).

SDSS-DR7, using SCAMP (Bertin et al. 2002). A 4 sigma-clipped median stacking is performed with SWarp (Bertin et al. 2002). The photometric catalog is then extracted with SExtractor (Bertin & Arnouts 1996), in dual-mode with the *i*-band as the detection image. Photo-z are computed with EASY (Brammer et al. 2008), using a prior on the redshift distribution at a given *i*-band magnitude from the semi-analytical model of Guo et al. (2011) and with zero-point (ZP) corrections applied (Lin et al. 2014). Two fields, MD04 (or PS1MD04) and MD07 (or PS1MD07), are selected as examples for this first study. PS1MD04 has a photo-z accuracy ~0.047 with a outlier rate 0.040 down to $i_{P1} < 22.5$. PS1MD07 has a photo-z accuracy ~0.051 with a outlier rate 0.074 down to $r_{P1} < 24.1$. The outlier rate is defined as the fraction of objects for which $| z_{phot} - z_s | > 0.15 \times (1 + z_s) \sim 3 \times \sigma_{\Delta z/(1+z_s)} \times (1 + z_s)$ for PS1 data, and the photo-z accuracy, $\sigma_{\Delta z/(1+z_s)}$, is estimated from the deviation of $| z_{phot} - z_s |/(1 + z_s)$ without the outliers. Two PS1 data sets are adopted to demonstrate the performance of PFOF with relatively "poor" photo-z accuracy.

Information from all data sets is summarized in Table 1.

3. METHOD

3.1. Probability Friends-of-Friends

PFOF was developed by Liu08 to identify galaxy groups and clusters in a galaxy catalog with redshift measurement errors. We briefly review the algorithm below, and readers are referred to Liu08 for a detailed discussion. PFOF is based on the FOF algorithm (Huchra & Geller 1982), modified to take into account photometric redshift uncertainty. Therefore, similar to the FOF algorithm, the criteria applied in PFOF to determine if two galaxies are physically linked are divided into two parts: the condition in the projected plane and in the line-of-sight direction. In the projected plane, the linking criterion is used to examine whether the separation of two galaxies, d_{12}, is less than the comoving linking length l_p, i.e., $d_{12} \leqslant l_p$, where l_p is a parameter. In the line-of-sight direction, given the photometric redshift probability distribution functions for the two galaxies G_1 and G_2, the probability P of the distance between them, which is less than the z-linking length, l_z, is defined as

$$P(|z_2 - z_1| \leqslant l_z) \equiv \int_0^\infty dz G_1(z) \int_{z-l_z}^{z+l_z} G_2(z')dz', \quad (1)$$

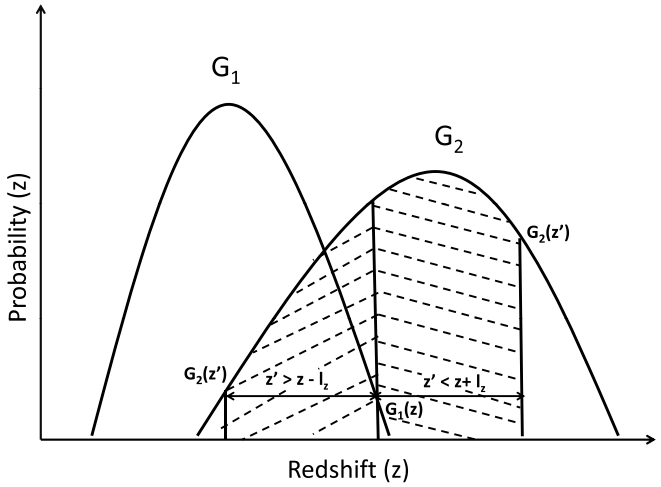

Figure 1. Schematic illustration of Equation (1), which expresses the probability of galaxies with photometric redshifts being separated by $|z_2 - z_1|$ which is less than the radial linking length l_z.

where l_z is the comoving linking length in the line-of-sight direction. The linking criterion then has to satisfy

$$P(|z_2 - z_1| \leqslant l_z) \geqslant P_{th}, \quad (2)$$

where P_{th} is a tunable linking probability threshold. When both criteria are satisfied, the two galaxies are called friends. The integration is described schematically in Figure 1. We continue searching for all the friends of one galaxy and then the friends of those friends, until finally a group is formed. In this way, given l_p, l_z, and p_{th}, PFOF constructs a list of group members. For a sample with a limiting magnitude, the mean density of galaxies n decreases with increasing redshifts, leading to a steady increase in the mean intergalaxy separation with z. To compensate for this effect, both l_p and l_z are expressed in terms of $n_0^{-1/3}$, where n_0 is the mean galaxy density, i.e.,

$$l_p(z) = b_p\, n_0(z)^{-1/3}, \quad (3)$$

and

$$l_z(z) = b_z\, n_0(z)^{-1/3}, \quad (4)$$

where b_p and b_z are dimensionless linking parameters perpendicular and parallel to the line of sight. Thus, the three adjustable parameters in the PFOF group finder are b_p, b_z, $P_{\rm th}$.

3.2. Purity and Completeness

To assess the performance of a group finder, two quantities, purity and completeness, can be adopted to characterize the overall fidelity of the resulting group catalogs, i.e., Eke et al. (2004). However, different definitions for purity and completeness can lead to distinct results. Our definitions for purity and completeness follow those of Gerke et al. (2005). In the following, we briefly explain the definitions used. For a more detailed discussion, the reader is referred to Gerke et al. (2005), Knobel et al. (2009), and Knobel et al. (2012). First, we define a "reconstructed group" (or a PFOF group) identified by our group-finder as a "pure group" when more than 50% of its members are associated with a "real group" (or a mock group) defined by the DM halos in the simulation. Conversely, in order for a "real group" to be a complete group, more than 50% of its members must be associated with a "reconstructed group." In addition, if a PFOF group is a pure group but its associated real group is not a complete group, and vice versa, the association is called a one-way match. If a PFOF group is a pure group and its associated real group is also a complete group, the association is called a two-way match. The purity and completeness of a group catalog can be defined according to the association as follows. For a one-way match,

$$p_1 = \frac{N_{\rm pure}}{N_{\rm PFOF}}, \tag{5}$$

and

$$c_1 = \frac{N_{\rm complete}}{N_{\rm real}}, \tag{6}$$

where $N_{\rm pure}$, $N_{\rm complete}$, $N_{\rm PFOF}$, and $N_{\rm real}$ are the number of pure groups, complete groups, PFOF groups (or reconstructed groups), and real groups, respectively. For a two-way match,

$$p_2 = \frac{N_2}{N_{\rm PFOF}} \tag{7}$$

and

$$c_2 = \frac{N_2}{N_{\rm real}}, \tag{8}$$

where N_2, is the number of pure and complete groups. Moreover, when a real group is identified as several smaller groups in the reconstructed catalog, the situation is called "fragmentation." Conversely, overmerging is when two or more real groups are identified as a single reconstructed object.

In practice, a perfect reconstructed group catalog is not achievable, with purity and completeness having a tendency to be mutually exclusive (e.g., Gerke et al. 2005; Knobel et al. 2009). A similar tension exists between overmerging and fragmentation. Some statistics introduced by Knobel et al. (2009) and Knobel et al. (2012) to measure "goodness" in such a way that maximizes (or minimizes) them yields a sort of "optimal" group catalog. In this study, we adopt three statistics from these works, g_1, g_2, and $\widetilde{g_1}$, for the purpose of our group catalog optimization. We briefly review these quantities here. The first quantity g_1 is defined as

$$g_1 = \sqrt{\frac{(1-p_1)^2 + (1-c_1)^2}{2}}, \tag{9}$$

which is normalized to be between 0 and 1. This is slightly different from the original g_1 definition in Knobel et al. (2009) and gives the distance to this optimal point in the c_1-p_1 plane; thus, this is a measure of the balance between completeness and purity. The second quantity g_2 is defined as

$$g_2 = \frac{c_2}{c_1}\frac{p_2}{p_1}, \tag{10}$$

and measures the balance between overmerging and fragmentation. The last quantity $\widetilde{g_1}$ has the form

$$\widetilde{g_1} = \sqrt{\frac{(1-p_2)^2 + (1-c_2)^2}{2}}, \tag{11}$$

which is similar to g_1 except that all one-way match statistics are replaced by their two-way match statistic counterparts. For a perfect group catalog, we expect that c1 $\simeq$ c2 $\simeq$ 1 and p1 $\simeq$ p2 $\simeq$ 1, meaning that essentially neither overmerging nor fragmentation is present in the catalog. Therefore, g_1 and $\widetilde{g_1}$ should approach 0 and g_2 should approach 1.

Since g_1 is based only on one-way match statistics, the resulting catalog, if optimized, might unnecessarily contain many such overmerged or overfragmented groups that will exhibit very good one-way statistics but very poor two-way statistics (Knobel et al. 2012). Instead of using g_1, we follow Knobel et al. (2012) and take $\widetilde{g_1}$ as the main optimization measure throughout this paper.

3.3. Subset Optimization

In addition to making use of the Durham mock catalog to optimize PFOF grouping, we alternatively optimize our linking lengths and threshold probability, i.e., l_p, l_z, and $P_{\rm th}$, by utilizing published spectral-z group catalogs as the training set. That is, zCOSMOS groups are the training set for PS1MD04 and DEEP2 groups for PS1MD07. In other words, we use spectral-z groups with a high sampling rate in the same field as the training set so as to avoid any dependence on the semi-analytical model, which may turn out to be an imprecise representation of the observational data. The optimization procedure is as follows. For a given set of linking lengths and thresholds, PFOF detects photo-z groups from a photometric galaxy sample. For a PFOF group, this may include galaxies with or without a spectroscopic redshift. We identify galaxies with spectral-z in the group to form a sub-group and then evaluate the purity and completeness of the sub-group with reference to published spectral-z groups to obtain the optimization measure $\widetilde{g_1}$. We survey a wide range of linking lengths and thresholds to locate the minimum value of $\widetilde{g_1}$ from the subsample as our optimization target. The main concern for this method is whether the optimal set of linking lengths and thresholds found from these sub-groups is also the optimal one for the full data set. To examine the feasibility of the method, we then use Durham mock catalog to simulate a sample with a 50% sampling rate similar to the zCOSMOS or DEEP2 surveys as the subsample, and test whether the two minimum $\widetilde{g_1}$'s from the subsample and from the full sample, have the same linking length and threshold.

4. PS1 MOCK GROUP CATALOG

For an FOF-based grouping algorithm, linking length calibration is important and necessary. Mock catalogs, in spite of their possibly inaccurate realization of the universe, can not only provide self-consistent tests but also serve as the tool for evaluating our training efficiency.

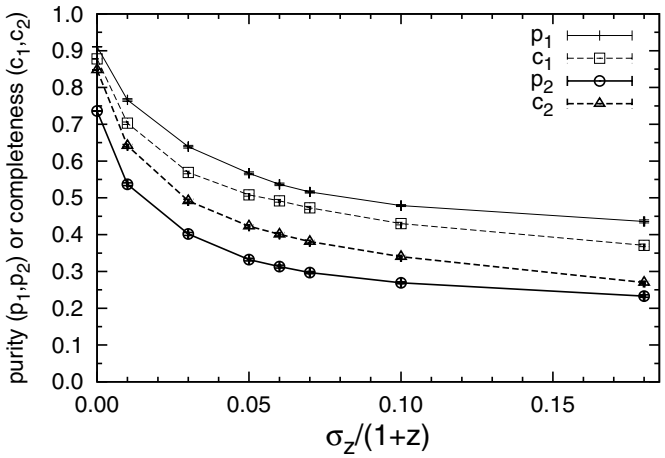

Figure 2. Purity or completeness is plotted as a function of photometric redshift accuracy $\sigma_{\Delta z/(1+z_s)}$. In the range of $\sigma_{\Delta z/(1+z_s)}$ between 0.03 and 0.07, purity or completeness drops by less than 20%. For current PS1 Medium Deep data, whose $\sigma_{\Delta z/(1+z_s)}$ is expected to be in the range between 0.03 and 0.07, the performance of the PFOF should not change dramatically. Error bars show the deviation over 50 realizations of the redshift errors.

4.1. Performance Dependence on Photometric Redshift Accuracy

To assess the dependence of the performance of PFOF on photometric redshift (or photo-z) accuracy, we apply PFOF to various simulated widths of photo-z error ranging from $\sigma_{\Delta z/(1+z_s)} = 10^{-4}$ to 0.2. We select galaxy samples with $i \leqslant 24.1$ and $z \leqslant 1.4$ and evaluate purity and completeness for groups with a richness of $N \geqslant 4$. For the photo-z simulation, we perturb the original observed redshift $z_{\rm obs}$ by adding an extra Gaussian distributed δz with variance of a given photo-z error $\sigma_{\Delta z/(1+z_s)}$. That is, the photo-$z$ uncertainties $\sigma_{\Delta z}$ are simulated to be scaled with $(1+z_s)$. Additionally, an outlier rate of 4% is considered in the photo-z simulation in the redshift range $0 < z < 1.4$. For a detailed discussion of the simulation of photo-z, see Liu08.

Figure 2 shows the result of the purity and completeness as functions of photo-z error, $\sigma_{\Delta z/(1+z_s)}$. The error bars show the 1σ deviation for 50 realizations. It can be seen that the purity and completeness drop when the photo-z error increases. This is expected since a large uncertainty in redshift makes group recovery more unreliable. In addition, the small error bars also indicate the stability of the PFOF algorithm. When varying $\sigma_{\Delta z/(1+z_s)} = 0.03$ to 0.07, p_1 and c_1 decline by $\sim$19% and $\sim$14%, respectively. Over this range of errors, the performance of PFOF does not change significantly. That is, PFOF performance is not sensitive to photo-z accuracy for a PS1 MDS-like survey where the expected photo-z accuracy falls into this range.

4.2. The Mock Group Catalog with $\sigma_{\Delta z/(1+z_s)} = 0.06$

The typical error width of photo-z accuracy $\sigma_{\Delta z/(1+z_s)}$, for five-band surveys such as Pan-STARRS Medium Deep Survey fields, is roughly 0.06 (Saglia et al. 2012). We shall illustrate the PFOF group finding results with this error using the mock catalog as follows. The selection cut for galaxies is the same as in the previous test and we focus on groups with a richness of $N \geqslant 4$. The values of p_1 and c_1 when the catalog is optimized are found to be 54% and 49%, respectively, after optimization.

Figure 3 shows a simple comparison between the PFOF and mock group catalogs by plotting both sets of clusters residing in halo masses of $M_h \geqslant 10^{14}\,h^{-1}\,M_\odot$ up to $z = 1.4$. Centers of open and solid circles with color-coded redshift represent the

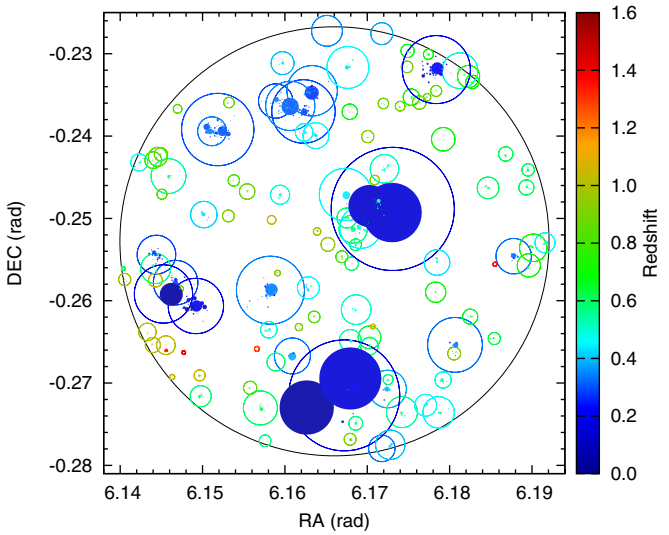

Figure 3. Distribution of PFOF and mock groups with halo masses $M_h \geqslant 10^{14}\,h^{-1}\,M_\odot$ in a simulated case with $\sigma_{\Delta z/(1+z_s)} = 0.06$. PFOF and mock groups with color-coded redshift are represented with solid and open circles, respectively, and with radii equal to the maximum center-to-member distance. The big black circle denotes the field of view of 7 deg^2, equivalent to a single pointing of PS1. It is seen that most of the mock groups are detected by PFOF groups ($\sim$97%), at roughly correct redshift, and that PFOF groups (solid circles) tend to have smaller sizes and be fragments of the corresponding mock groups. (A color version of this figure is available in the online journal.)

positions of the mock and PFOF groups and their radii give the maximum group member distance from the group center. The big black circle gives the field of view of 7 deg^2, equivalent to a single pointing of PS1. It can be seen that most mock groups are detected by PFOF (112 out of 116), where the successful detection is to recover a minimum of five member galaxies from the mock groups, and these PFOF groups are at roughly the correct redshift. However, the mock groups appear to be fragmented by the PFOF detection. To quantify the grouping performance, we follow the work of Murphy et al. (2012) and plot the color-coded purity and completeness as functions of dark matter halo mass M_h and redshift z with sampling intervals of 0.05 in redshift and 0.2 in $\log_{10}$ halo mass. We also smooth the data using a 3×3 grid in redshift and log mass bins, for which the purity or completeness of a given cell is the mean value over this coarse region, and set a threshold of at least five clusters detected in this region. In Figure 4, p_1 (top) and c_1 (bottom) are shown. It can be seen that for high masses ($M_h \geqslant 10^{14}\,h^{-1}\,M_\odot$), the recovered groups are highly pure but not compete, consistent with the result from Figure 3. The opposite trend can be seen between purity and completeness, i.e., the highly complete region has low purity. Note that the high purity and low completeness in the high halo mass region seem to disagree with the averaged values of p_1 and c_1 when the catalog is optimized, being equal to 54% and 49%, respectively. This is mainly due to the fact that the averaged values of p_1 and c_1 are global measures, derived by optimization over all $N \geqslant 4$ groups; the abundant low N groups dominate the global measures and compromise the high-mass-end results.

In addition, we note that performance based on purity and completeness can vary significantly with their definitions. In the following, we adopt the definitions of purity and completeness from the ORCA method of Murphy et al. (2012) to illustrate the dependence of performance on the definitions. For an ORCA complete group, a halo is detected if at least $N_{\rm min}$ galaxies

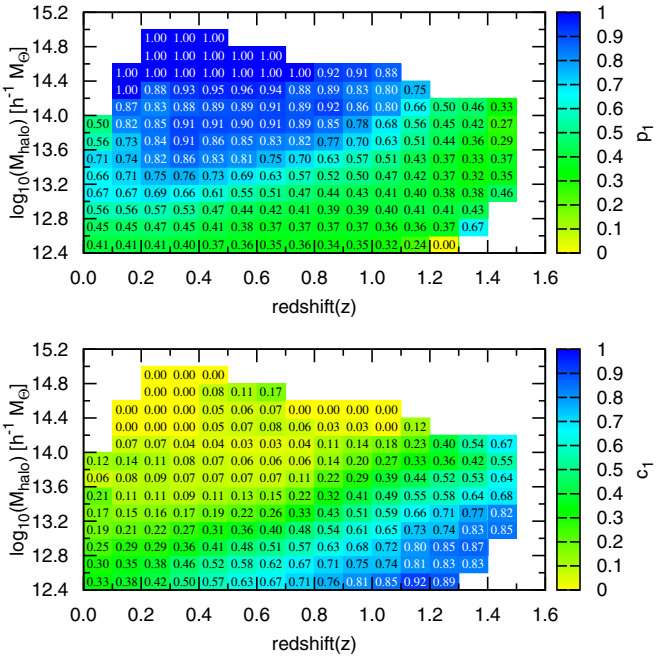

Figure 4. Color-coded purity p_1 (top) and completeness c_1 (bottom) are plotted as a function of redshift z and halo mass M_h. This plot is an illustration of the grouping result with parameters optimized for the low richness groups. In the high mass range $\sim 10^{14}\,h^{-1}\,M_\odot$, PFOF groups are pure and their corresponding mock groups are incomplete, consistent with what we see in Figure 3. By contrast, in lower-mass halos ($\log_{10} M_h < 13.2$) and higher redshift ($z > 0.8$) ranges, the opposite result is obtained in that PFOF groups are not pure and their corresponding mock groups are more complete. The low completeness for high-mass halos is mainly due to optimization over all $N \geqslant 4$ groups, which dominate the global measures.

(A color version of this figure is available in the online journal.)

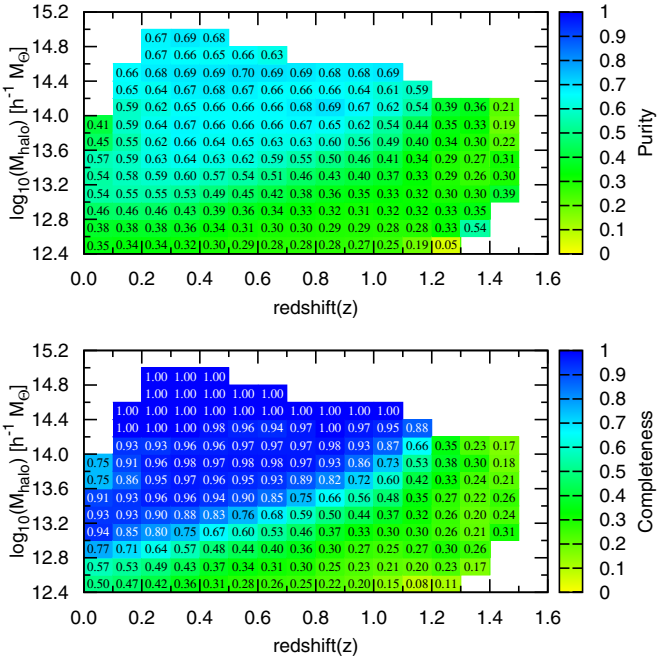

Figure 5. Purity (top) and completeness (bottom) computed as defined by Murphy et al. (2012) are displayed as a function of z and M_h to illustrate that for the same PFOF group catalog, depending on the definition of purity or completeness used, the PFOF performance can change appreciably.

(A color version of this figure is available in the online journal.)

are identified, even if they are shared between multiple ORCA clusters. In ORCA, purity is defined as the fraction of galaxies assigned to the group that are members of the host halo. With the same group catalog used previously for p_1 and c_1 in Figure 4, we plot the purity (top) and completeness (bottom) with the ORCA definition in Figure 5 to demonstrate the difference. For the purity comparison, the difference is small. This is simply because two purity definitions are close to each other. ORCA purity drops slightly compared to PFOF purity. However, for completeness, the discrepancy between the two definitions is large. The original low completeness in the high mass region in PFOF definition becomes high completeness with the ORCA definition while the original high completeness in the low mass region using the PFOF definition becomes lower completeness in the ORCA definition.

To elaborate on the difference caused by two definitions, an explicit example is illustrated as follows. Assuming that a real (or mock) group has 10 members, corresponding to this real group there are 3 groups detected by PFOF with 7, 6, and 4 members, respectively. In these three PFOF groups, four out of seven, four out of six, and one out of four are real group members. In this case, two are pure groups and one is not in the PFOF definition. The PFOF purity is thus $2/3 \sim 0.66$, and, by contrast, the ORCA purity is $(4/7 + 4/6 + 1/4)/3 \sim 0.5$. On the other hand, there is no complete group in the PFOF definition, and the PFOF completeness is 0 while there are nine real members detected, which are larger than the threshold $N_{\rm min} = 5$, and the ORCA completeness hence is 1. From the above example, it is seen that two definitions lead to similar purities but significantly different completenesses.

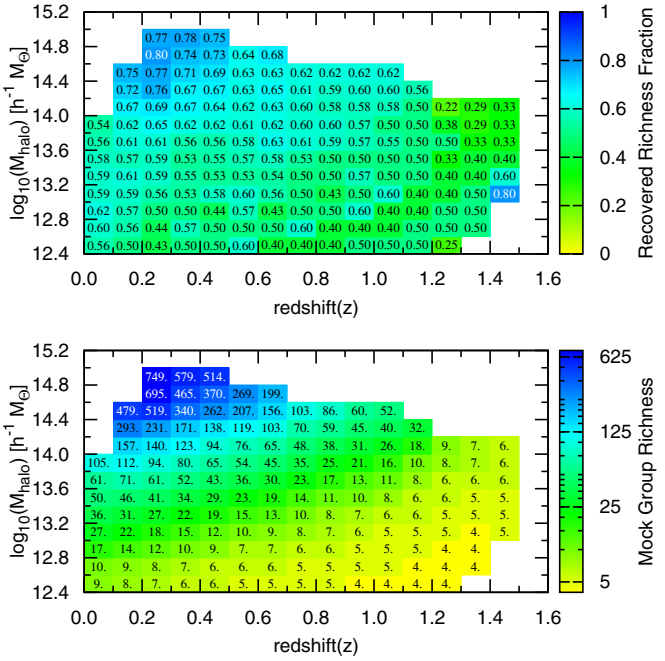

Figure 6. Recovered richness fraction from PFOF groups (top) and original richness from their corresponding mock groups (bottom) are shown in terms of z and M_h. PFOF groups compose $\gtrsim$60% of members from their original mock groups with high richness, $N \geqslant 10$. For a fixed richness, the distribution of the richness is a linear function of z and M_h, and this is due to a limiting magnitude selection for the sample.

(A color version of this figure is available in the online journal.)

Finally, we address the richness recovery. For comparison, the richness of mock data (bottom) and the recovered richness fraction of PFOF (top) groups are plotted in terms of halo mass M_h and redshift z in Figure 6. The recovered richness is defined

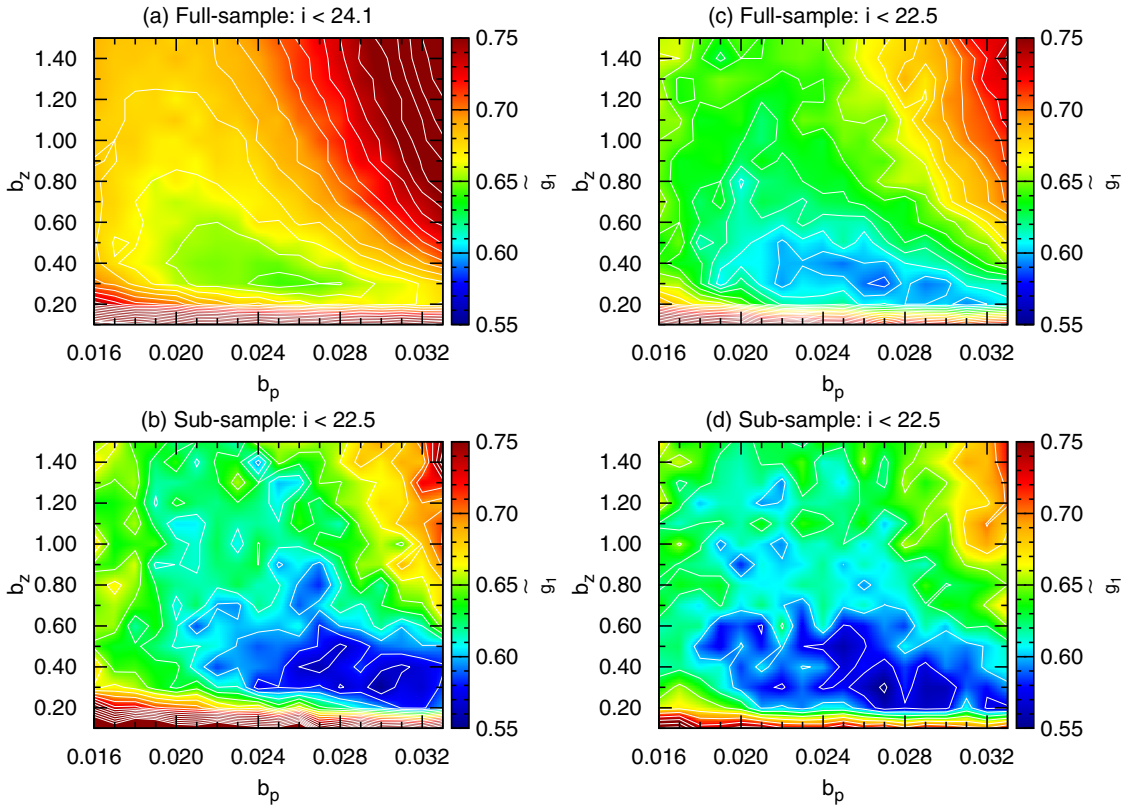

Figure 7. Optimization measure $\tilde{g_1}$ is plotted as a function of linking length parameter parallel (b_z) and perpendicular (b_p) to the line of sight at a fixed threshold, $p_{\rm th}$. To simulate the survey sampling rate and area of zCOSMOS, we randomly select 50% of galaxies from the Durham mock in 2 deg^2 as the subsample. In addition, we consider one case with the same magnitude cut ($i \leqslant 22.5$) for both full (c) and subsample (d), and the other one with a different magnitude cut applied to the full (a) ($i \leqslant 24.1$) and subsample (b) ($i \leqslant 22.5$). In both two cases, the simulated photo-z accuracy 0.06 is applied. It is found that in both cases the minima of $\tilde{g_1}$ from the full sample and the subsample coincide with each other, i.e., the optimal set of linking lengths and threshold selected from the subsample are the same as in the full sample. Therefore, subset optimization is feasible.

(A color version of this figure is available in the online journal.)

as the richness sum of PFOF groups corresponding to the same mock group and the correspondence is assured by the one-way match criterion. It is found that PFOF can detect $\gtrsim$60% of the members from high richness groups, $N \geqslant 10$. In other words, at a specified M_h and z, the recovered richness is $\sim$25% less than mock group richness. Additionally, for the same richness, groups are more massive at higher redshift due to the applied limiting magnitude selection. We test using the method of rank-ordering richnesses to recover the richness (and hence mass). This works properly for the high richness groups. However, as the richness lowers, fragmentation, overmergers, and/or false detection destroy the correspondence, resulting in the wrong mass estimation. We find that for the halo mass $>10^{14}\,h^{-1}\,M_\odot$, the offset is -0.26 dex and the scatter is 0.47 dex, and for the halo mass $>10^{13}\,h^{-1}\,M_\odot$, the offset is -0.33 dex and the scatter gets worse, becoming 0.72 dex.

4.3. Depth and Absolute Magnitude Selection

To understand how the depth of a sample affects our group finder performance, we select a sample with $i \leqslant 25.8$ and a simulated photo-z width $\sigma_{\Delta z/(1+z_s)} \sim 0.06$ in the redshift range between 0 and 1.4 for PFOF grouping. We obtain the values of $p_1 = 51\%$ and $c_1 = 45\%$ when the catalog is optimized, which are $\sim$8% lower than those found for a sample with a shallower depth $i \leqslant 24.1$. It appears that the worse performance is due to poor photo-z for faint galaxies, and for PFOF grouping, increasing depth thus leads to a worse performance. However, this effect is not significant.

Similarly, a sample based on a restframe magnitude selection is also set up to probe the group finding performance. A sample is selected with z up to 1.4 with an absolute magnitude cut of $i \leqslant -19.0$, corresponding to roughly the similar galaxy number density as that in the sample with a flux-limit $i \leqslant 24.1$ plus a simulated photo-z width of $\sigma_{\Delta z/(1+z_s)} \sim 0.06$ to search for the optimal grouping performance. The values of p_1 and c_1 are 62% and 61% at the minimal $\tilde{g_1}$, respectively. Compared to that of the flux-limited sample, the performance has a roughly 20% increase.

4.4. Subset Optimization Study

In this section, we make use of the Durham mock catalog to set up two cases for studies of the subset optimization. In the first case, we select 50% of galaxies with $i \leqslant 22.5$ in a 2 deg^2 field to be our subsample to mimic the roughly 50% sampling completeness case, e.g., 20 k zCOSMOS galaxies in PS1MD04. For the full sample, two different photometric depths, $i \leqslant 24.1$ and $i \leqslant 22.5$, are applied. When we look for optimal linking lengths and thresholds, we find that the minimal $\tilde{g_1}$, the optimization measure, is located at $P_{\rm th} = 0.001$. To illustrate how the optimization measure evolves with linking length, we plot the color-coded $\tilde{g_1}$ at fixed $P_{\rm th} = 0.001$ as a function of linking parameters perpendicular and parallel to the line of sight, b_p and b_z, over-plotted with $\tilde{g_1}$ contours in Figure 7. The left two

panels show results for the full sample (upper) with a depth of $i \leqslant 24.1$ (1) and for the subsample (lower) with $i \leqslant 22.5$ (2), while the right two panels are also for the full sample (upper) (3) and for the subsample (lower) (4) but both have a depth $i \leqslant 22.5$. That is, there is a depth difference between the full sample and the subsample (the left two panels) but no depth difference between the right two panels. It can be seen that from the left two panels, there are two comparable local minimal $\tilde{g_1}$'s in the subsample. One matches the minimum in the full sample, but the other deviates from that in the full sample, which turns out to be one of the local minima with $\tilde{g_1}$ close to the global minimum. Therefore, if we identify the optimal linking lengths using a subsample with a certain depth difference from its full sample, it seems that the shorter optimal linking lengths are likely to be the correct optimal linking lengths. On the other hand, from the right panels the two minima are located at roughly the same linking lengths, meaning that we can find the real optimal linking lengths for the full sample via "subset optimization."

In the other case, we select 50% of galaxies with $i \leqslant 24.1$ in a 1 deg^2 field to be our subsample to mimic roughly 50% of sampling completeness for DEEP2 EGS galaxies in PS1MD07. The same depth as in the subsample is set for the full sample. Similar to Figure 7, we also plot the optimization measure $\tilde{g_1}$ at fixed $P_{\rm th} = 0.001$ in Figure 8. The result shows that the minimum in the subsample can match that in the full sample at the same linking lengths. We thus conclude that the survey area of the subsample does not appear to be a relevant factor.

As we know, the spectroscopic sample is in general brighter than the photometric sample. Therefore what we want to test with the mock catalogs is to what extent the linking length trained with a brighter (shallower) sample can be applied to a deeper survey. To do that, we constructed two training samples (subsamples) with different depths (shallow versus deep). What we found was that the PFOF performance in the case of using the shallower training set is as good as in the case of using the deeper training set. In other words, by optimizing the recovering rate for brighter group members in the subsample, we are also allowed to optimize the recovering rate for the fainter group galaxies in the full sample containing fainter galaxies. Therefore, our conclusion from this test is that a spectroscopic sample with a shallow depth compared to its associated photo-z survey is sufficient to be a training sample for the PFOF optimization. On the other hand, from the observational point of view, a shallow spectroscopic survey is easier to achieve than a deep one. This makes the optimization of PFOF easy to apply to observation data.

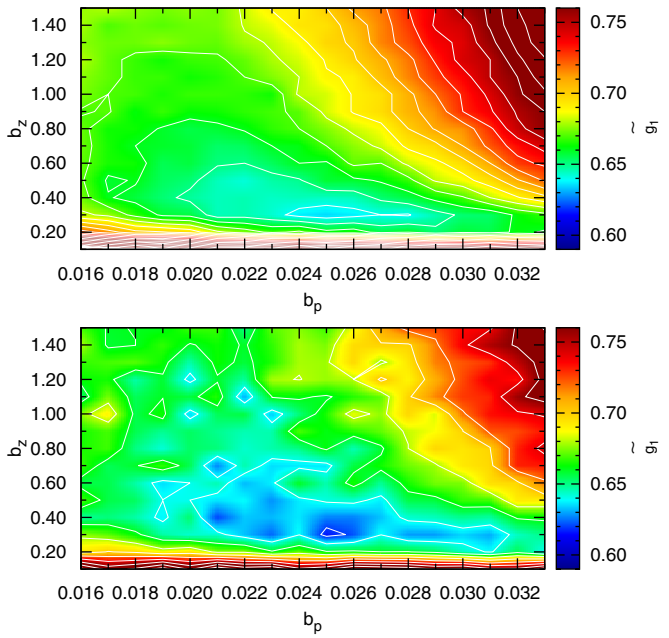

Figure 8. Similar to Figure 7. We simulate the survey sampling rate (∼50%) and area (∼1 deg^2) similar to the DEEP2 EGS using the Durham mock catalog. We again find that the optimal set of linking lengths and threshold with the minimum $\tilde{g_1}$ found from the subsample are the same as those derived from the full sample.

(A color version of this figure is available in the online journal.)

5. OBSERVATIONAL DATA APPLICATIONS

In this section, we utilize four observational data sets, including photometric galaxy catalogs of COSMOS, EGS, PS1MD04, and PS1MD07, to illustrate the grouping performance of PFOF via a subset optimization for various photo-z error widths, $\sigma_{\Delta z/(1+z_s)} = \sim 0.01$ (COSMOS), 0.03 (EGS), and 0.06 (PS1MD04 and PS1MD07), respectively. For PFOF grouping, the minimum richness cut for a subsample and full sample are 3 and 4, respectively.

5.1. COSMOS Group Catalog

We make use of the public COSMOS galaxy catalog (George et al. 2011) for PFOF group finding. In this catalog, the typical redshift accuracy can reach $\sigma_{\Delta z/(1+z_s)} \lesssim 0.007$ for galaxies with F814W < 22.5, and $\sigma_{\Delta z/(1+z_s)} = 0.012$ for F814W $= 24$, at $z < 1.2$ (Ilbert at al. 2009). The catalog contains 115,831 galaxies with F814W < 24.2 up to $z \sim 4.6$, and the survey area is ∼2-deg^2. We focus on galaxies below redshift 1.4. In total we obtain 104,060 galaxies in the full sample. In addition, we take the zCOSMOS 10 k group galaxies (Knobel et al. 2009) to be our subsample. There are 11,262 zCOSMOS galaxies with $z < 1.4$ and $i \leqslant 22.5$ in the area of 2 deg^2.

Via the subset optimization, we obtain overall values of $p_1 = 74\%$ and $c_1 = 69\%$ at the minimal $\tilde{g_1}$ from the zCOSMOS subsample with the linking probability threshold $P_{\rm th} = 0.04$ and the redshift dependent comoving linking lengths parallel and perpendicular to line-of-sight, l_p and l_z, between 0.10 and 0.55 Mpc for $l_p(z)$ and between 3.4 and 19.06 Mpc for $l_z(z)$. PFOF reconstructs 212 groups in the zCOSMOS subsample, which originally had 226 spectral-z groups. On the other hand, PFOF also detects a total of 3,314 groups in the full COSMOS sample, with 20,954 group galaxies (∼20.2% of the original galaxy sample). In Figure 9, we plot PFOF groups in the subsample using solid circles and zCOSMOS groups with open circles with color-coded z and radius, the maximum member-group center distance, in the redshift range $0 < z < 1.2$. We compute p_1 and c_1 in six redshift bins, (1) $0 < z < 0.2$, (2) $0.2 < z < 0.4$, (3) $0.4 < z < 0.6$, (4) $0.6 < z < 0.8$, (5) $0.8 < z < 1.0$, and (6) $1.0 < z < 1.2$. The result can be found in Table 2. We also can observe some fragmented and overmerged subgroups from PFOF detections but the fragmentation and overmerger problems are not serious.

To assess the performance of membership identification from PFOF, we compare our COSMOS group galaxies to X-ray membership galaxies from George et al. (2011). We find that the photo-z dispersion from PFOF group galaxies is slightly smaller than that from X-ray cluster galaxies. Thus PFOF performance is comparable to that of other group finders.

Table 2
Grouping Performance $p_1(z)$ and $c_1(z)$

Catalog Name	$0 < z < 0.2$ p_1/c_1	$0.2 < z < 0.4$ p_1/c_1	$0.4 < z < 0.6$ p_1/c_1	$0.6 < z < 0.8$ p_1/c_1	$0.8 < z < 1.0$ p_1/c_1	$1.0 < z < 1.2$ p_1/c_1
COSMOS	0.83/0.55	0.75/0.66	0.84/0.79	0.66/0.73	0.60/0.67	N/A
EGS	0.0/0.0	0.65/0.65	0.57/0.50	0.56/0.82	0.650/0.44	0.25/0.50
PS1MD04	0.57/0.07	0.56/0.22	0.53/0.61	0.55/0.62	0.26/0.68	0.50/0.50
PS1MD07	1.0/0.0	0.71/0.30	0.49/0.44	0.51/0.63	0.52/0.54	0.48/0.77

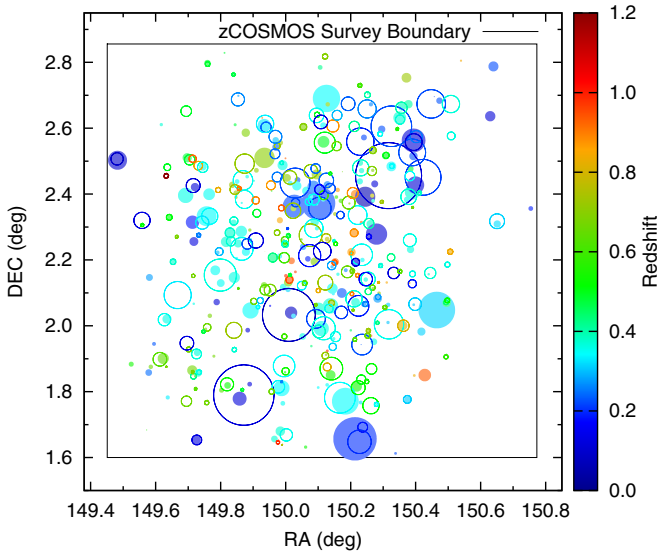

Figure 9. Distribution of PFOF COSMOS subgroups (solid) and zCOSMOS groups (open) with color-coded redshift and radius equal to maximum center-to-member distance in the redshift range $0 < z < 1.2$. We obtain the values of $p_1 = 74\%$ and $c_1 = 69\%$ when the catalog is optimized.

(A color version of this figure is available in the online journal.)

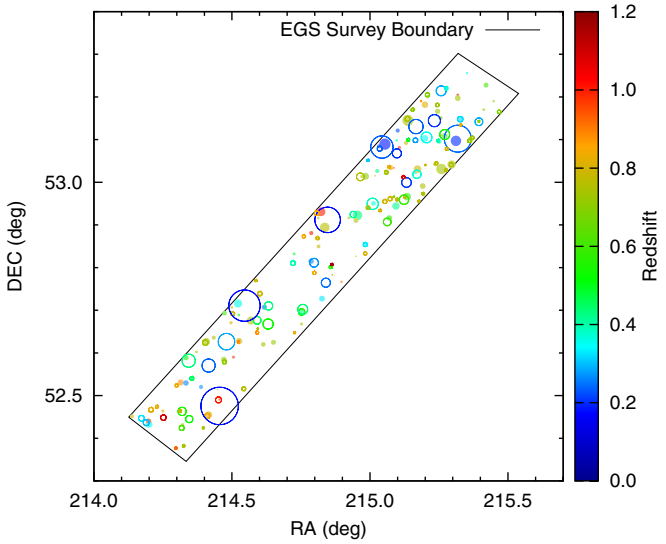

Figure 10. Distribution of PFOF EGS subgroups (solid) and DEEP2 EGS groups (open) with color-coded redshift and radius equal to maximum center-to-member distance. For this case, we obtain the values of $p_1 = 55\%$ and $c_1 = 61\%$ from the subsample when it is optimized.

(A color version of this figure is available in the online journal.)

5.2. EGS Group Catalog

In the EGS photometric galaxy sample, we have the same selection cut for galaxies, with $R \leqslant 24.1$ and photo-z up to 1.4, and obtain 8,558 galaxies and 3,526 galaxies to be the input full sample and subsample, respectively. After optimization, we find that the values of p_1 and c_1 at the $\widetilde{g_1}$ are 55% and 61% from the subsample with $p_{\rm th} = 0.01$, $l_p(z) = 0.32$ to 0.57 Mpc, and $l_z(z) = 3.84$ to 6.94 Mpc. In the subsample, there are 96 spectral-z groups, and PFOF identifies 103 subgroups while in the EGS full sample, 218 groups ($N \geqslant 4$) are detected and they contain 1,213 group galaxies (∼14% of the EGS sample). Similar to Figure 9 but without redshift binning, the location, color-coded redshift, and radius of 96 DEEP-EGS (solid circle) and 103 PFOF (open circle) subgroups are plotted in Figure 10 in six redshift ranges of equal partition between $z = 0$ and 1.2 and the result is shown in Table 2.

5.3. PS1MD04 Group Catalog

In PS1MD04, we again utilize zCOSMOS 10 k groups as the subsample for subset optimization. We apply the same selection cut, where $i_{\rm P1} \leqslant 24.1$ and photo-$z \leqslant 1.4$, to the PS1MD04 catalog, and acquire 345,446 and 9,557 galaxies for the full sample and subsample, respectively. The values of p_1 and c_1 at the $\widetilde{g_1}$ from the subsample are found to be 49% and 45% with $p_{\rm th} = 0.001$, $l_p(z) = 0.20$ to 0.66 Mpc, and $l_z(z) = 0.36$ to 1.15 Mpc. We identify 293 PFOF subgroups from the zCOSMOS subsample which has 227 groups, and in total, detect

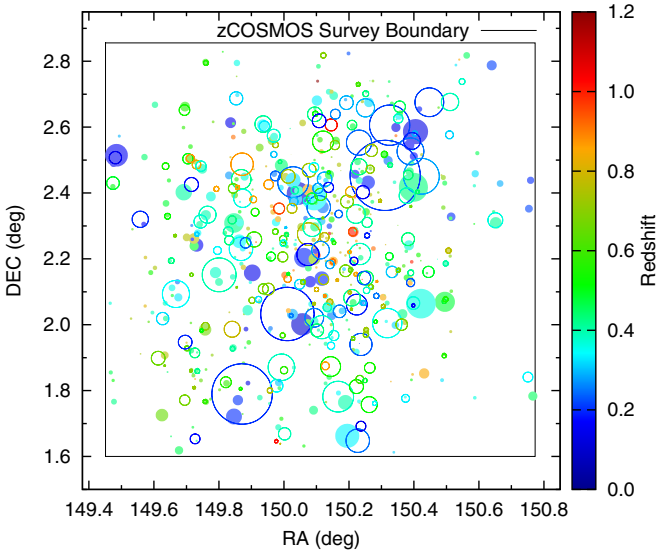

Figure 11. Similar to Figure 9, we plot the distribution of PFOF PS1MD04 subgroups (solid) and zCOSMOS groups (open) with color-coded redshift and radius equal to maximum center-to-member distance. For this case, the values of $p_1 = 49\%$ and 45% at the minimal $\widetilde{g_1}$ are obtained when the catalog is optimized.

(A color version of this figure is available in the online journal.)

9,318 groups in PS1MD04 and 59,997 group galaxies, roughly 17.4% of PS1MD04 sample. In Figure 11, we plot the result of our subgroup finding by splitting it into six redshift bins as we did in Figure 9. The result is summarized in Table 2.

Table 3
Grouping Results

Catalog Name	$l_p(z)$ (Mpc)	$l_z(z)$ (Mpc)	$p_{\rm th}$	p_1	c_1	Density ($N \geqslant 4$) deg^{-2}	Offset $\Delta z_p^{\rm Grp}$	Scatter $\sigma_{\Delta z^{\rm Grp}/(1+z_s^{\rm Grp})}$
COSMOS	$0.10 \sim 0.55$	$3.40 \sim 19.06$	0.04	0.74	0.69	1.84×10^3	−0.009	0.021
EGS	$0.32 \sim 0.57$	$3.84 \sim 6.94$	0.01	0.55	0.61	4.22×10^2	−0.005	0.032
PS1MD04	$0.20 \sim 0.66$	$0.36 \sim 1.15$	0.001	0.49	0.45	1.53×10^3	0.010	0.045
PS1MD07	$0.12 \sim 0.36$	$0.56 \sim 1.71$	0.001	0.53	0.46	1.70×10^3	0.003	0.048

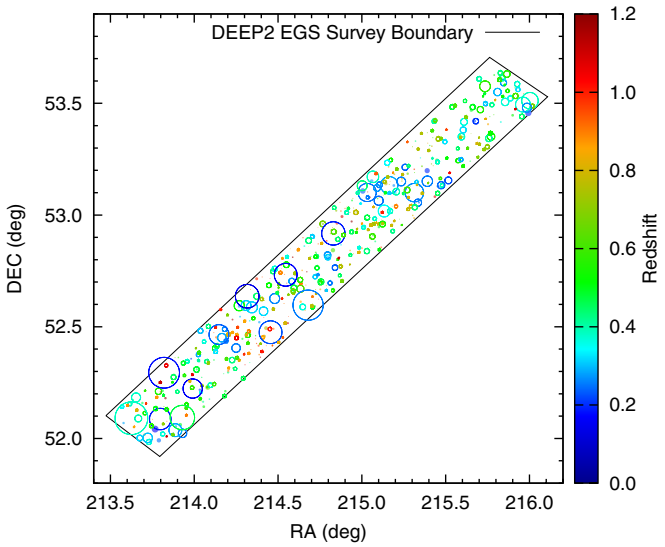

Figure 12. Similar to Figure 10, distribution of PFOF PS1MD07 subgroups (solid) and DEEP2 EGS groups (open) is plotted with color-coded redshift and radius equal to maximum center-to-member distance. In this case, we get the values of $p_1 = 53\%$ and $c_1 = 46\%$ when the catalog is optimized.
(A color version of this figure is available in the online journal.)

5.4. PS1MD07 Group Catalog

In PS1MD07, DEEP2-EGS groups are adopted again as the subsample. A selection cut is applied, with $i_{\rm P1} \leqslant 24.1$ and photo-$z \leqslant 1.4$, to the catalog, and we obtain 479,200 and 11,194 galaxies for the two samples. The values of p_1 and c_1 at the $\widetilde{g_1}$ from the subsample are found to be 53% and 46% with $p_{\rm th} = 0.001$, $l_p(z) = 0.12$ to 0.36 Mpc, and $l_z(z) = 0.56$ to 1.71 Mpc. We reconstruct 319 PFOF subgroups from the DEEP2-EGS subsample (originally 326 groups) as plotted in Figure 12, and in total, detect 13,784 groups and 76,155 group galaxies in PS1MD04, roughly 16% of the PS1MD07 sample. In the six redshift ranges, the performance is listed in Table 2.

The PFOF grouping results and the performance as a function of redshift for the four data sets are summarized in Table 3.

5.5. Estimation on the Recovering and Contamination Rate for Red and Blue Group Galaxies of PFOF

It is well known that the accuracy of photo-z is correlated with the colors of galaxies, and therefore we now turn to discussing how well PFOF can recover blue and red group galaxies by using the EGS described in Section 5.2 and the PS1MD07 group catalog in Section 5.4, respectively. We select PFOF group galaxies with spectral-z in groups with richness $N \geqslant 4$ and redshift between 0.5 and 1.0, and also identify their corresponding spectral-z groups and group galaxies in these corresponding spectral-z groups to obtain the recovery rate as a function of color. We find that in terms of rest-frame $U-B$ color or $(U-B)_0$, where galaxies with $(U-B)_0 \geqslant 0.9$ are red and others are blue, in the EGS group catalog, PFOF recovers 43 red and 99 blue spectral-z group galaxies from the original 63 red and 147 blue DEEP2 EGS group galaxies, and the recovery rate for red and blue galaxies in groups are 68.3% and 67.3%, respectively. Similarly, in the PS1MD07 group catalog, we find that the recovering rate for red galaxies is 73.6% (89/121) and for blue ones is 71.5% (264/396). In other words, PFOF detection is not biased toward blue or red galaxies. This demonstrates that PFOF does not have a preferential color selection for identifying a galaxy as a group member. The ratio of red to blue group galaxies is ∼0.27 in EGS and ∼0.28 in PS1MD07. We also compute the contamination rate in terms of color for PFOF group galaxies with spectral-z in groups with a richness $N \geqslant 4$ and a redshift between 0.5 and 1.0. In the EGS group catalog, we find that for red galaxies, 32 out of 75 (∼42.7%) galaxies in PFOF group galaxies with spectral-z are actually field galaxies according to the DEEP2 group catalog, and for blue, 143 out of 242 (∼59.1%) are field galaxies. On the other hand, in the PS1MD07 group catalog, the contamination rate for red galaxies is ∼55.5% (111/200) and for blue ones it is ∼66.8% (532/796). That the contamination rate is less for red galaxies is expected due to better photo-z for red than for blue galaxies in general.

The spectral-z samples used in this paper as the training sets are mainly from the DEEP2 survey with a magnitude cut of $R < 24.1$ and the zCOSMOS sample with i < 22.5. The two samples may be biased toward emission-line galaxies in particular in the faint end regime where the red galaxies do not have enough signal-to-noise ratio in the absorption features. On the other hand, due to the poorer photo-z accuracy for blue galaxies compared to red ones, a training sample that contains more blue galaxies may be helpful for calibrating the group finder parameters. There is probably no perfect solution for a training sample to get rid of such bias. PFOF is inevitably also affected by the training sample bias. However, depending on the science goals, one can use different samples for the training purpose when applying PFOF. Optimizing the parameters to recover the blue group members is one of the strengths of PFOF, unlike many other group-finding methods that are biased toward red galaxies. Ideally, we may take into account the selection function of individual galaxies in the spectroscopic sample by giving the weighting when doing the optimization. The main purpose of this paper is to demonstrate the performance of PFOF, and we thus assume no selection effect in the subsamples.

5.6. Chance Associations and Redshift Precision of PFOF Groups

To assess the grouping effect caused by the chance associations, a random catalog is created by completely scrambling positions while other properties are fixed. PFOF is then applied on the random catalog using the same optimized linking lengths

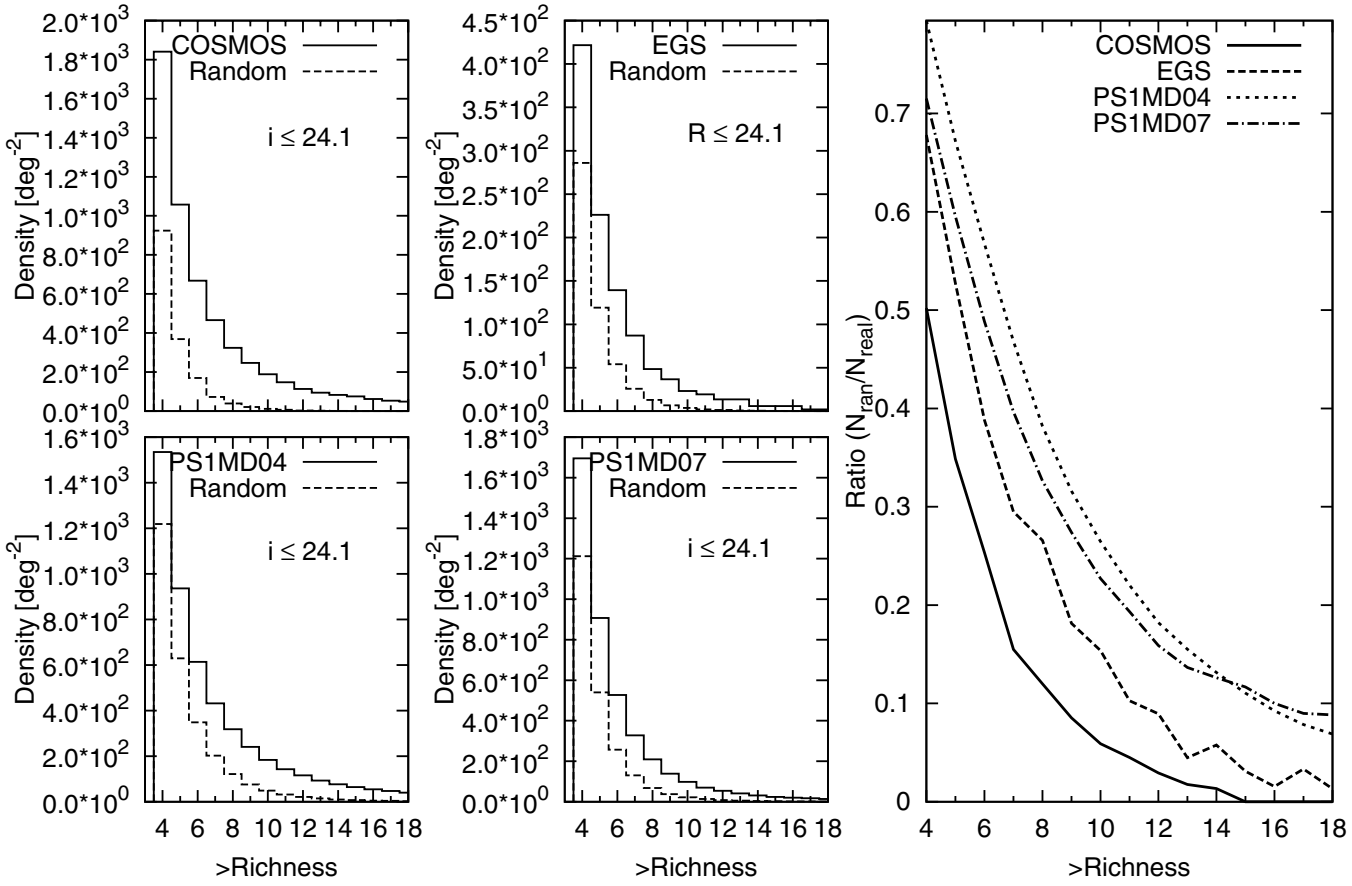

Figure 13. On the left four panels, the space density of groups detected in our four data sets and in their corresponding random catalogs is plotted as a function a threshold richness. The random catalogs are created by completely scrambling the positions while keeping other properties fixed. In the EGS field, the flux limit cut we set is $R = 24.1$ different from the flux limit cut $i = 24.1$ in the other catalogs. On the right panel, the ratio of the random group density to the PFOF group density is plotted as a function a threshold richness. A larger richness cut is necessary for a catalog with poor photo-z performance to achieve the same ration as in a catalog with better photo-z performance.

and threshold from the corresponding field. We measure the group density of the random and PFOF groups as a function of the threshold richness and compute the ratio of the random group density to the PFOF group density. From the left four panels in Figure 13, the density is plotted as a function of threshold richness. It is seen that the density of PFOF groups is much less in EGS than that in the other three fields. The density of the PFOF groups differs across different samples; this is due to the different flux-limit cuts employed. From the right panel in Figure 13, the ratio of the random group density to the PFOF group density is also plotted as a function of threshold richness. We find that the ratio correlates with photo-z accuracy. As the photo-z performance degrades, the richness cut has to increase to maintain a fixed ratio of the group number from the random catalog to the real group number. For example, at a ratio of 20%, it is required to have $N \geqslant 7$ for COSMOS, $N \geqslant 9$ for EGS, $N \geqslant 11$ for PS1MD07, and $N \geqslant 12$ for PS1MD04. That is, comparing to the good photo-z catalog, i.e., the COSMOS catalog, the poor photo-z catalog, i.e., the PS1MD04 or PS1MD07 catalog, needs a larger richness cut to reduce the effect caused by the chance associations. The low significance in PS1MD04 (the red line) in Figure 15 appears to be caused by the high proportion of chance associations for the richness cut 4. In addition, we also find that the significance is ∼4.3 for the COSMOS group catalog and ∼1.6 for PS1MD04 when referenced to its scrambled random catalog, consistent with the significance results in Section 5.7.

The redshift precision of the reconstructed groups is also an important issue to be addressed. In Figure 14, we plot spectral-z $z_s^{\rm Grp}$ versus photo-z $z_p^{\rm Grp}$ for the matched groups (top) and the redshift difference between photo-z and spectral-z ($\Delta z^{\rm Grp} = z_p^{\rm Grp} - z_s^{\rm Grp}$) for the matched groups as a function of $z_s^{\rm Grp}$ (bottom) in (1) COSMOS, (2) EGS, (3) PS1MD04, and (4) PS1MD07. We find that the offset $\langle \Delta z^{\rm Grp} \rangle$ and scatter $\sigma_{\Delta z^{\rm Grp}/(1+z_s^{\rm Grp})}$ in (1) COSMOS are −0.009 and 0.021, in (2) EGS −0.006 and 0.032, in (3) PS1MD04 0.010 and 0.045, and in (4) PS1MD07 0.003 and 0.048. As expected, the scatter of the group redshift difference correlates with the photo-z performance of the catalog. A catalog with a worse photo-z performance results in a larger scatter of the redshift difference among group members.

5.7. Comparisons to the X-Ray Catalog in the COSMOS Field

To further assess the PFOF performance, we compare our group catalogs in the COSMOS field, i.e., the COSMOS and PS1MD04 catalogs, to the *XMM-Newton* plus *Chandra* X-ray catalog (George et al. 2011) in the same field, and compute the number of matched PFOF detected groups as a fraction of the number of the X-ray clusters. The criteria for a successful match (or detection) are that the center of a PFOF group has to be inside r_{200} of an X-ray cluster, the radius within which the mean density is 200 times the critical density of the universe at the redshift of the group, and that the redshift difference between a

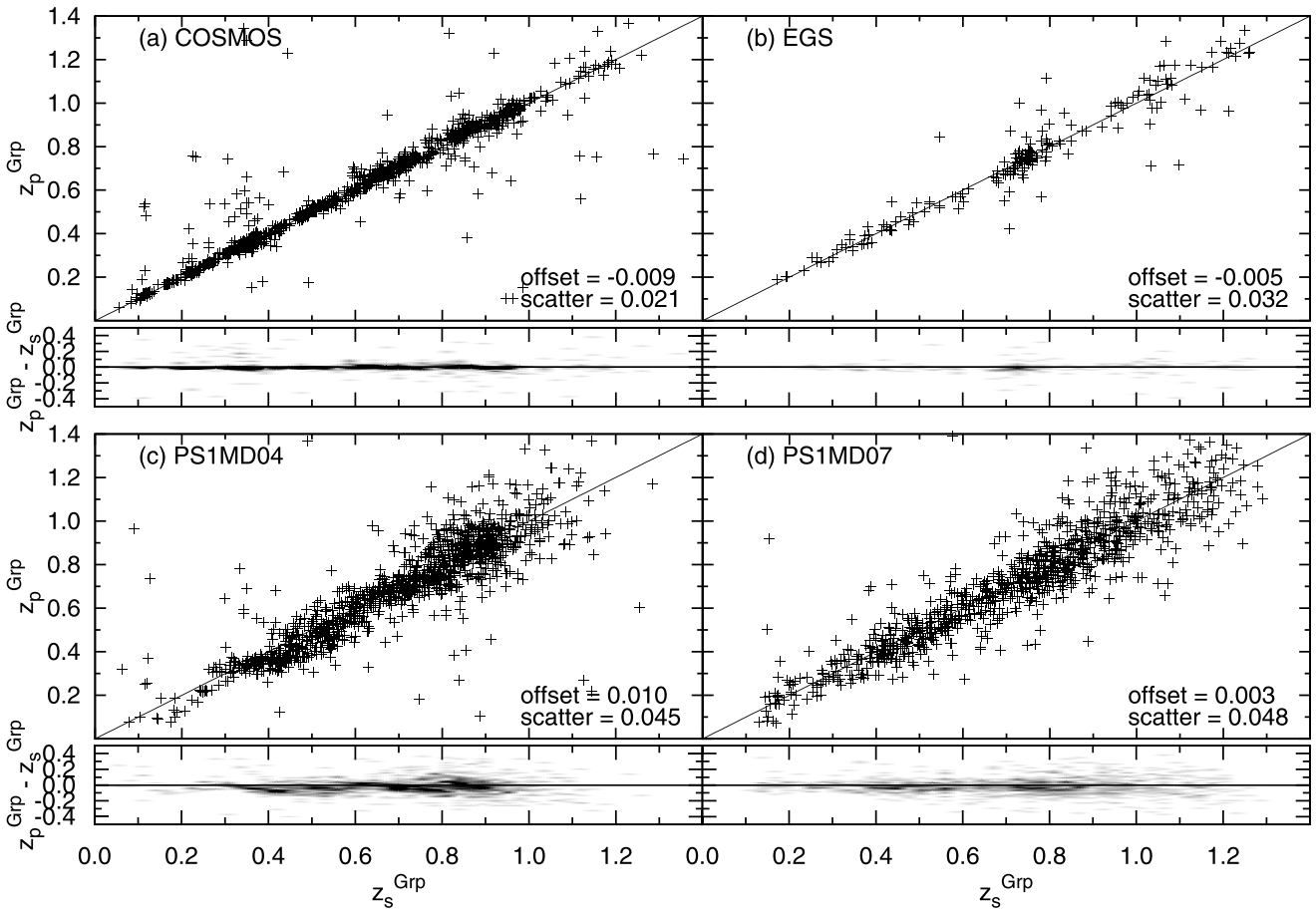

Figure 14. Spectral-$zz_s^{\rm Grp}$ vs. photo-$zz_p^{\rm Grp}$ for the matched groups (top) and the redshift difference between photo-z and spectral-z ($\Delta z^{\rm Grp} = z_p^{\rm Grp} - z_s^{\rm Grp}$) for the matched groups as a functions of $z_s^{\rm Grp}$ (bottom) are plotted for (a) COSMOS, (b) EGS, (c) PS1MD04, and (d) PS1MD07.

PFOF group and an X-ray cluster is within $1.5\sigma_{\Delta z/(1+z_s)}$, where $\sigma_{\Delta z/(1+z_s)}$ is the photo-z uncertainty width of a sample. The factor of 1.5 is an adjustable value roughly to allow for those groups with worse redshift identification to have a successful matching. In addition, to know whether the match occurs by chance, we construct a random catalog by randomly distributing the position of X-ray clusters but keeping their original redshifts and r_{200}, and examine the match between PFOF and the random catalog. We repeat the procedure 50 times and average over the matched fractions, and then define the significance as the ratio of the matched fraction from the X-ray catalog to the average fraction from the random catalogs to understand the effect of coincidence. When the significance is equal to 1, it implies that the match with the X-ray catalog may be totally caused by chance. On the other hand, when the significance is high, it indicates that the purity of the group catalog is also likely to be high. In Figure 15, we plot the matched fraction (upper) for PS1MD04 with $N \geqslant 4$ (red), PS1MD04 with $N \geqslant 7$ (black), COSMOS (blue), and zCOSMOS (green) and significance (lower) as functions of the threshold mass of M_{200} of X-ray clusters using the zCOSMOS catalog as the reference. From Figure 15, it can be seen that the matched fraction of the three catalogs remains roughly constant as the value of M_{200} decreases, indicating that our detections for low mass X-ray clusters do not decrease significantly. Despite the higher matched fraction ∼87% from the PS1MD04 catalog with $N \geqslant 4$ compared to the COSMOS matched fraction (∼85%), its matched fraction to the random catalog is also significantly high (∼54%), and hence its significance turns out to be the lowest (∼1.5), implying that the high photo-z uncertainty (or a looser constraint in redshift difference) causes more X-ray detections by chance. Alternatively, we use the PS1MD04 catalog with $N \geqslant 7$ for the X-ray matching. This catalog results in a better significance over 3, though its completeness ∼70% is relatively lower than the case with $N \geqslant 4$. While the matched fraction from the COSMOS catalog is ∼85% and significance is ∼5.0 times higher than expected for random matches, the zCOSMOS catalog shows much lower matched fraction of ∼60% but even higher significance ∼25. A loosening of the constraints in the criterion of redshift difference introduces a higher random matched fraction, and thus higher false detection rates. It thus follows that the photo-z accuracy has a significant impact on the group finding. Moreover, we find that the low matched fraction ∼60% from the zCOSMOS catalog mainly results from the problems of its survey incompleteness, in some areas at lower redshift that accounts for the unmatched fraction of ∼13%, and for the flux-limited, high redshift groups that accounts for ∼29%. Furthermore, both PFOF COSMOS and PS1MD04 catalogs also have matched fractions close to their respective maximum matched fractions, 89.9 and 91.4%, suggesting that our subset optimization is successful.

In Figure 15, the low significance ∼1.6 seems to imply a poor performance in the PFOF grouping. However, it is worth noting that the matched fraction and significance depend on the richness cut. The example shown in Figure 15 is to demonstrate that a high matched fraction (∼85%) can be achieved by adopting

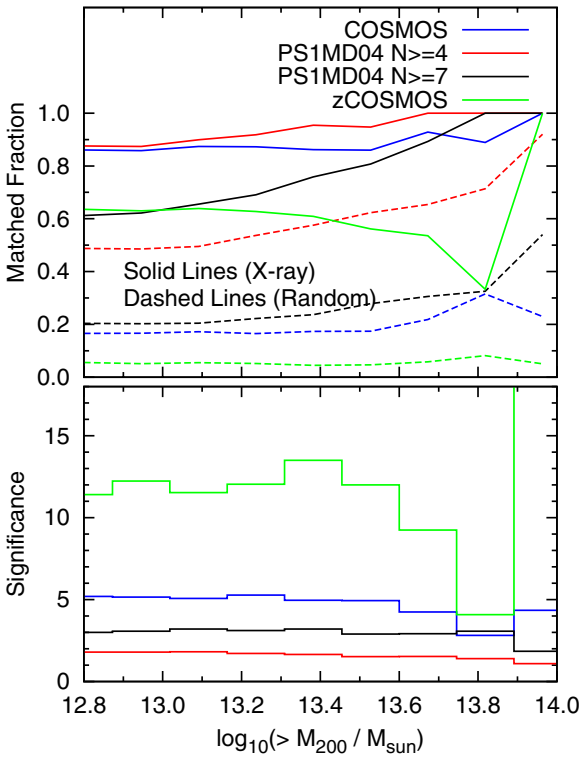

Figure 15. Matched fraction (top) and significance (bottom) are plotted as a function of threshold $\log_{10}(M_{200}/M_{\odot})$ for the case using zCOSMOS groups as the training set, where the significance is defined as the ratio of the matched fraction from the X-ray catalog to the average fraction from the random catalogs. The dashed lines give the matched fraction from random catalogs. It is seen that the matched fraction is ∼85% for COSMOS and 87% for PS1MD04 when the richness threshold is 4. The higher matched fractions from PSMD04 are due to a looser constraint on the redshift difference compared to that from COSMOS to include many false detections of low richness groups, leading to a lower value of significance. To make a meaningful catalog for PS1MD04, a proper richness threshold has to be set to remove those false detections although a lower completeness of the X-ray clusters is obtained. For example, when $N \geqslant 7$ for PS1MD04 (the black lines), the matched fraction drops to ∼70% but the significance can reach ∼3.

(A color version of this figure is available in the online journal.)

a low richness cut $N \geqslant 4$ with the trade off of high false associations. Nevertheless, the PFOF group catalog can still be useful for sciences by applying a higher richness cut. For example, when we set the richness cut $N \geqslant 7$ for the MD04 groups, we would obtain a lower matched fraction ∼70% but a much higher significance ∼3. In this case, the catalog may be more appropriate for science. This approach is demonstrated in Lin et al. (2014), who selected groups with richness $10 < N \leqslant 25$, and clusters with $N \geqslant 25$. Small richness groups are neglected due to lots of false detections. When studying the galaxy properties and the group and cluster environment, they calibrated the recovering and contamination rate of blue and red group galaxies using the spectral-z group information, as discussed in Section 5.5. That is, by properly calibrating the field contamination and group incompleteness, the properties of the group galaxies can be recovered, making the scientific study available.

We also plot the location, angular size, and redshift of X-ray clusters (open circles) and zCOSMOS groups (solid circles) from zCOSMOS catalog Knobel et al. (2012) in (1), from PFOF COSMOS catalog in (2), and from PFOF PS1MD04 catalog in (3), respectively, in Figure 16 to demonstrate the detail of matched results. The angular size for the X-ray clusters is R_{200} and is the maximum member-group center distance for PFOF groups. From the map in (1), it is not surprising that the matched zCOSMOS groups have sizes comparable to X-ray clusters. Comparing results between the two different photo-z samples, i.e., (2) and (3), groups in PS1MD04 have more fragmentation. This implies that to acquire a higher matched fraction, PFOF groups tend to be more fragmented. This is because overmergers can often yield group positions departing from their real locations but also include too many false members to have group redshifts deviating from their real redshifts.

Ebeling et al. (2013) recently presented the results of a pilot study for the extended MACS survey (eMACS), which aims to expand the MACS cluster survey to higher redshift and lower X-ray fluxes by combining the two large-area imaging data sets introduced in the preceding sections: the ROSAT All-Sky Survey (RASS), including Bright and Faint Source Catalogs (BSC and FSC), and the PS1 3π survey. They apply no additional constraints regarding X-ray flux, spectral hardness ratio, or photon statistics and lower the redshift threshold to $z > 0.3$ to extend the probed luminosity range to poorer systems. Examination of PS1/MDS images for 41 BSC and 200 FSC sources combined with dedicated spectroscopic follow-up observations results in a sample of 11 clusters with estimated or spectroscopic redshifts of $z > 0.3$. Among those clusters, RXJ0959.0+0255 (gri, $z = 0.3494$) is in PS1MD04, and eMACSJ1419.2+5326 (riz, $z = 0.6384$) is in PS1MD07, and we thus use them to check PFOF identifications in these two fields. Figure 17 shows the rgb PS1 image (z-band for red, r-band for green, and g-band for blue) around RXJ0959.0+0255 and the PFOF detected group which has a mean photo-z redshift $z \sim 0.43$ in PS1MD04. The white circles denote PFOF group galaxies, the blue circle indicates the BCG of the group, the large white circle corresponds to a radius of $1\,h^{-1}$ Mpc, and red squares are spectral-z galaxies. Similar to Figure 17, Figure 18 shows the image around eMACSJ1419.2+5326, the PFOF detected group which has a mean photo-z redshift $z \sim 0.69$ in PS1MD07. In these two cases, both clusters are detected by PFOF. It is demonstrated again that PFOF is capable of finding clusters even for surveys with relatively "poor" photo-z accuracy, such as the PS1 survey.

In addition, the sample X-ray group, RXJ0959+0255, has a PFOF photo-z of 0.425, which is quite different from the spectroscopic redshift of 0.35. There are six PFOF group galaxies that match with the spectral-z galaxies in the X-ray cluster. We measure the offset and scatter for these six galaxies. We find that the scatter ∼0.039 of this particular cluster is in agreement with the scatter ∼0.045 for all groups as shown in Figure 14(c), but the offset ∼0.09 is larger and significantly deviates from the offset ∼0.01 in Figure 14(c). Such systematic offset is also seen in the spectral-z versus photo-z plot for PS1 galaxies in general, regardless of whether they belong to groups or not (Lin et al. 2014); a hump is present at $z \sim 0.35$. This suggests that the photo-z of the MD04 catalog at $z_s \sim 0.35$ is subject to larger uncertainty which leads to the overestimation of the photo-z of cluster RXJ0959+0255.

5.8. Discussion

The fact that we obtain both the purity and completeness are ∼85% for the richness $N \geqslant 4$ when applying PFOF on the zCOSMOS or DEEP data (the pure spectral-z data) does not necessarily disagree with the lower matching rate of

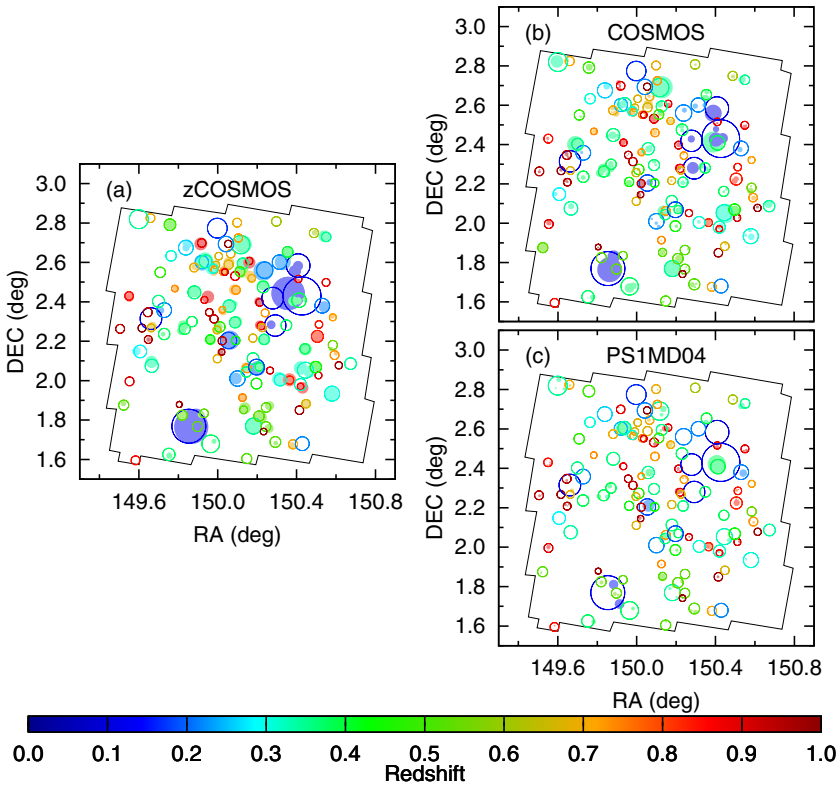

Figure 16. Distribution of matched PFOF groups and X-ray clusters is plotted with color-coded redshift and radius equal to maximum center-to-member distance. The black solid line gives the X-ray survey boundary. The open circles denote the X-ray clusters while the solid circles represent the PFOF groups. The radius of circles is equal to the maximum center-to-member distance. The left panel is for zCOSMOS (a), results from COSMOS and PS1MD04 are plotted in (b) and (c), respectively, using zCOSMOS as the training set. Comparing (c) to (b), X-ray clusters tend to be fragmented by PS1MD04 groups more than by COSMOS groups.
(A color version of this figure is available in the online journal.)

∼50% when matching two catalogs with noise in their richness estimates results as pointed out by Bahcall et al. (2003). In Bahcall et al. (2003), the matching is performed on two group catalogs with richness above a certain threshold. The matching is unsuccessful if a group in one catalog is below the threshold while in the other catalog it is above the threshold. On the other hand, in our case, the spectral-z group catalog is treated as the reference answer, and we do not apply any threshold cut on it in the matching process. In other words, the richness threshold cut is only applied to the PFOF groups. As a result, the values of the purity and completeness quoted in this work would have been greater than that if we were to adopt a similar approach defined by Bahcall et al. (2003). However, what we would like to demonstrate in this work is how the purity and completeness change with the photo-z inaccuracies. That is, the relative values of purity or completeness under conditions of different photo-z errors are more meaningful. In addition, due to the nature of our algorithm, we need a reference catalog to train our linking parameters. The spectral-z catalog probably is the best one can use as a reference membership catalog as long as the redshift completeness is high enough although scatter exists between spectroscopic samples. We stress that our catalog is tuned based on a specific spectral-z catalog hence the membership may be subject to a small change when different reference spec-z catalogs are adopted.

The photo-z accuracy in four galaxy samples varies from 0.01 to 0.05. With such a wide range of photo-z accuracy, there is no reason to have similar optimal linking lengths across the data sets. Particularly, we find that when the catalog is optimized, the parameter $p_{\rm th}$ in PFOF is coupled with the photo-z accuracy of that catalog. That makes the optimized linking lengths deviate significantly. To be fair, the comparison of the linking lengths should be made between the PS1MD04 and PS1MD07 catalogs due to their similar photo-z performance. However, the resultant optimized linking lengths in PS1MD04 turn out to deviate from those in PS1MD07. This is mainly because we adopt the different training set in PS1MD04 and PSMD07. Each training set has its own characteristics and properties, and we are thus biased to that training set when we try to recover it. A better way to check whether our algorithm is fundamentally stable or not is to apply the optimized linking parameters (not physical linking lengths) obtained from one field to the other field, i.e., from MD07 to MD04. This is the second optimization strategy, different from the strategy applied in Sections 5.1–5.4. We compare the number density in this MD04 catalog to the MD07 catalog as a function of redshift and richness in Figure 19. It is found that the number density distributions as a function of redshift or richness in these two fields are similar, implying the PFOF algorithm is stable. We also evaluate the performance of this MOD4 catalog by using the zCOSMOS groups catalog and the x-ray cluster catalog as the reference catalogs. We find that the matched fraction for the catalog is ∼91% and p_1, c_1, and $\widetilde{g_1}$ are 0.38, 0.42, and 0.66, close to the catalog with the minimum $\widetilde{g_1}$ 0.64 where p_1 is 0.49 and c_1 is 0.37. In addition, we also find that the optimized linking lengths from MD07 give $\widetilde{g_1}$ at the local minimum in MD04 and close to the absolute minimum 0.64. In other words, these two combinations of linking lengths (one from MD04 and the other from MD07) give nearly the same performance. It is thus concluded that the PFOF algorithm is stable.

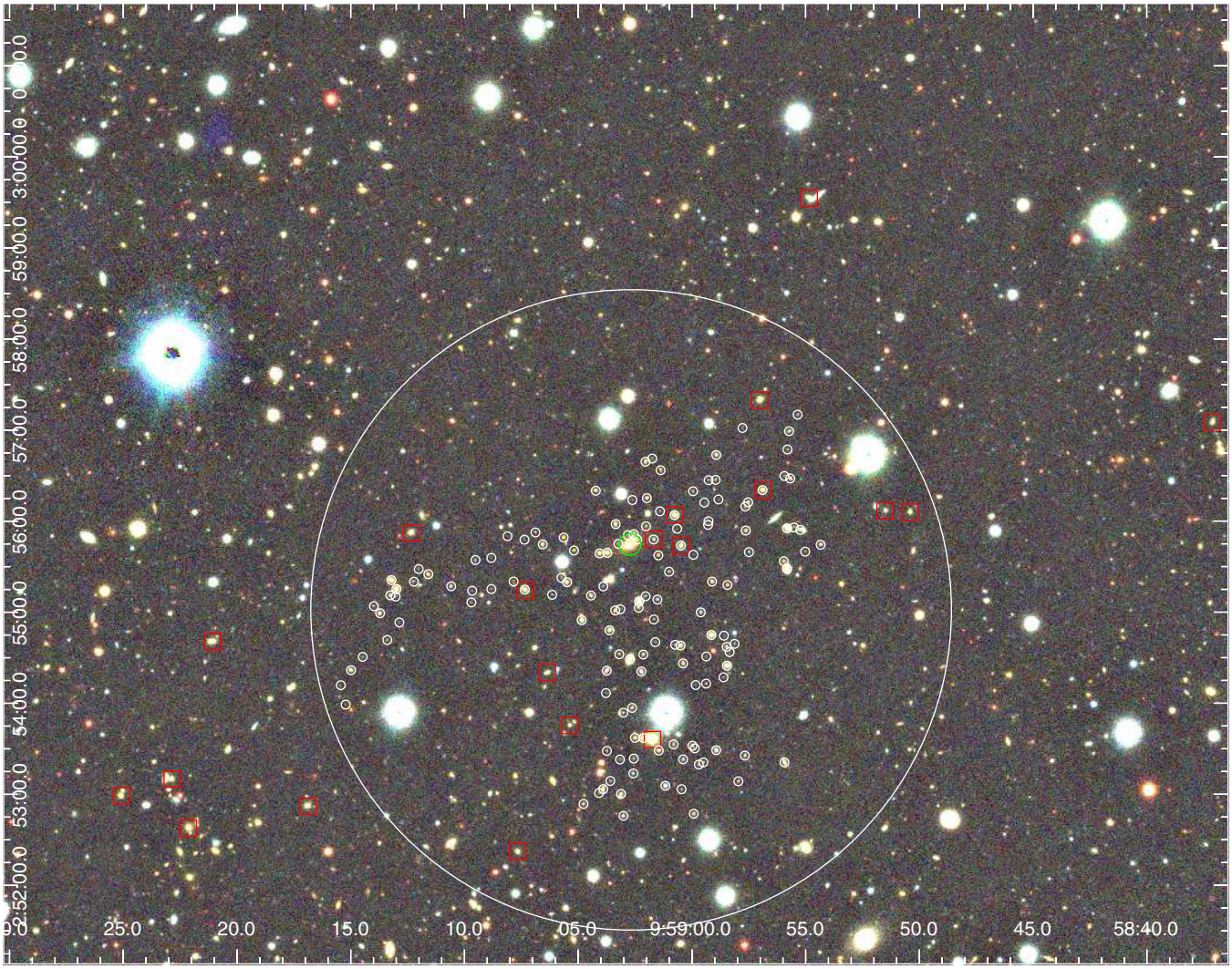

Figure 17. RXJ0959.0+0255. A PS1 image shows a PFOF detection ($z = 0.425$) in PS1MD04 on top of an X-ray cluster position ($z = 0.3494$). Members are marked in white while the BCG is indicated by the green circle. In addition, the larger white circle corresponds to $1\,h^{-1}$ Mpc based on the cluster redshift, and spectral-z galaxies are denoted by red squares in z range between 0.345 and 0.355. The map size is $\sim 13\farcm4 \times 10\farcm5$.

(A color version of this figure is available in the online journal.)

6. SUMMARY

We extend analyses of the PFOF group finder from the previous paper of Liu et al. (2008). We start by briefly reviewing the PFOF algorithm and then illustrating definitions of purity and completeness in PFOF. We adopt an optimization measure $\widetilde{g_1}$ introduced by Knobel et al. (2012). With the Durham mock catalog for the Pan-STARRS Medium Deep Survey, we demonstrate PFOF performance for various photo-z accuracies. In addition, to reduce any dependency of our group catalogs on the details of the mock catalogs, we adopt a calibration method, called subset optimization, by using spectroscopically identified groups from observational data as a training set to optimize PFOF grouping. The method is examined by using the mock catalog with a similar sampling rate and is shown to be feasible. We then apply subset optimization to observational data sets, considering photo-z accuracies ranging from "good" $\sigma_{\Delta z/(1+z_s)} \sim 0.01$ in COSMOS, to "medium" $\sim$0.03 in EGS, to relatively "poor" $\sim$0.06 in PS1MD04 and PS1MD07, to illustrate the performance of the PFOF in terms of photo-z accuracy. Moreover, we also match PFOF groups to *XMM-Newton* X-ray clusters to have an alternative performance check. In the end, we estimate the recovering rate for red and blue group galaxies to demonstrate that PFOF is not biased by color. Our results are summarized as follows.

1. To assess how PFOF performance varies with photo-z accuracy $\sigma_{\Delta z/(1+z_s)}$, we make use of the Durham mock catalog with simulated photo-z to study the purity and completeness as a function of $\sigma_{\Delta z/(1+z_s)}$ as shown in Figure 2. We find that purity or completeness drops by only $\sim$20% when $\sigma_{\Delta z/(1+z_s)}$ deteriorates from 0.03 to 0.07, to the expected range of redshift accuracy for PS1 photo-z.
2. Using a simulated $\sigma_{\Delta z/(1+z_s)} \sim 0.06$ with a selection cut, where $i \leqslant 24.1$, $z \leqslant 1.4$, and richness $N \leqslant 4$, as an example, we illustrate the performance of the PFOF in detail. For this case, the values of p_1 and c_1 are 54% and 49% at the minimal $\widetilde{g_1}$, respectively. We plot spatial distribution of PFOF groups overplotted with mock groups for halo masses $M_h > 10^{14}\,h^{-1}\,M_\odot$ in Figure 3. It is found that PFOF detects 112 out of 116 mock clusters with roughly correct redshifts, where a successful detection is to have at least five member galaxies from the mock groups. The four undetected clusters are at high redshift ($z > 1$) and

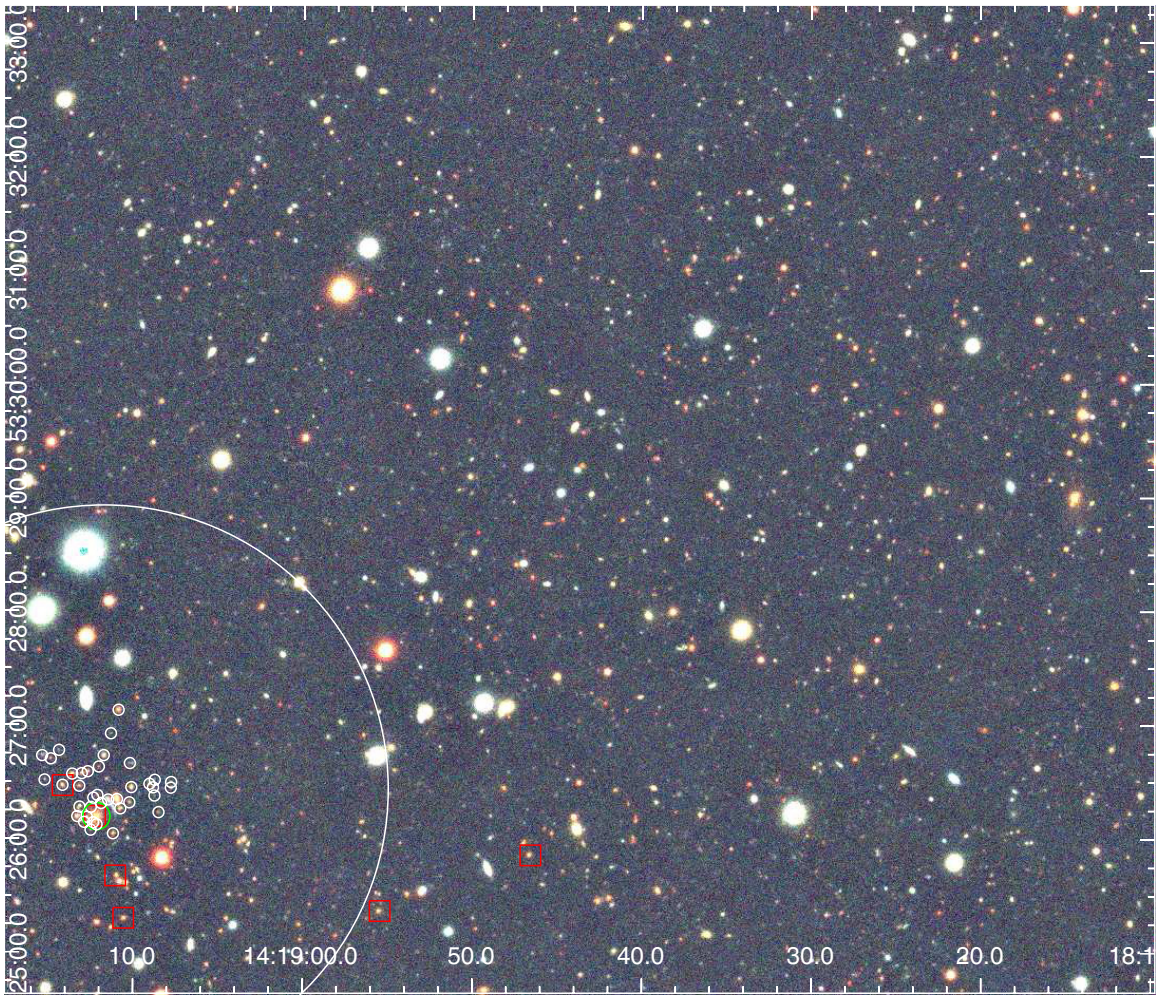

Figure 18. eMACSJ1419.2+5326. Similar to Figure 17, but a PFOF detection ($z = 0.687$) in PS1MD07 on top of an X-ray cluster position ($z = 0.6384$), and spectral-z galaxies (red squares) are in z range between 0.631 and 0.645. The X-ray cluster is on the corner of skycell 80. The map size is $\sim 16\farcm9 \times 8\farcm6$.

(A color version of this figure is available in the online journal.)

are low richness groups ($N \leqslant 5$). In addition, it is found that clusters tend to be fragmented by PFOF, i.e., 116 mock clusters fragmented into 875 PFOF groups, leading to a condition with high purity but low completeness.

3. When purity p_1 and completeness c_1 are expressed in terms of redshift z and halo mass M_h in Figure 4, we find that in the high mass range, PFOF groups are pure, but their corresponding mock groups are not complete, consistent with results described in (2). On the other hand, at lower M_h and higher z, we have the opposite trend where mock groups are more complete but their corresponding PFOF groups are less pure. The high purity and low completeness in the high halo mass region seem to disagree with the values of p_1 and c_1 at the minimal $\widetilde{g_1}$ mainly because the abundant low N groups dominate the global measures and compromise the high-mass-end results.
4. In addition to the definition we adopt for purity p_1 and completeness c_1 (Gerke et al. 2005, 2012; Knobel et al. 2009, 2012), we also use the definition adopted in ORCA (Murphy et al. 2012) for purity, which is defined as the fraction of galaxies assigned to the cluster that are members of the host halo. For a complete group, a halo is detected if at least $N_{\rm min}$ galaxies are identified, even if they are shared between multiple ORCA clusters. We adopted these definitions to demonstrate that for the same group catalog, performance based on different definitions can vary significantly.
5. From the mock test, when we increase the sample depth from 24.1 to 25.8 for PFOF grouping, the performance does not decrease significantly, only by $\sim$8%. When we adopt an absolute magnitude cut instead of a limiting magnitude cut for the same number density, we can increase the performance by $\sim$20%.
6. We develop an optimization method, called the subset optimization, for PFOF, and make use of the mock catalog to simulate two different cases to test the idea and demonstrate from both cases that the optimal linking lengths and threshold obtained from the subsample coincide with those obtained from the full sample. In other words, subset optimization is a feasible methodology.
7. By using the 10 k zCOSMOS groups as the training set, the purity p_1 and completeness c_1 from the subsample are 74% and 69% at the minimal $\widetilde{g_1}$ for COSMOS galaxies with "good" photo-z accuracy $\sim$0.01, and are 49% and 45% for PS1MD04 with poorer photo-z accuracy $\sim$0.05.
8. By using the DEEP2 EGS groups to train the linking lengths, we obtain the values of $p_1 = 55\%$ and $c_1 = 61\%$ at the minimal $\widetilde{g_1}$ for the EGS catalog with "medium" photo-

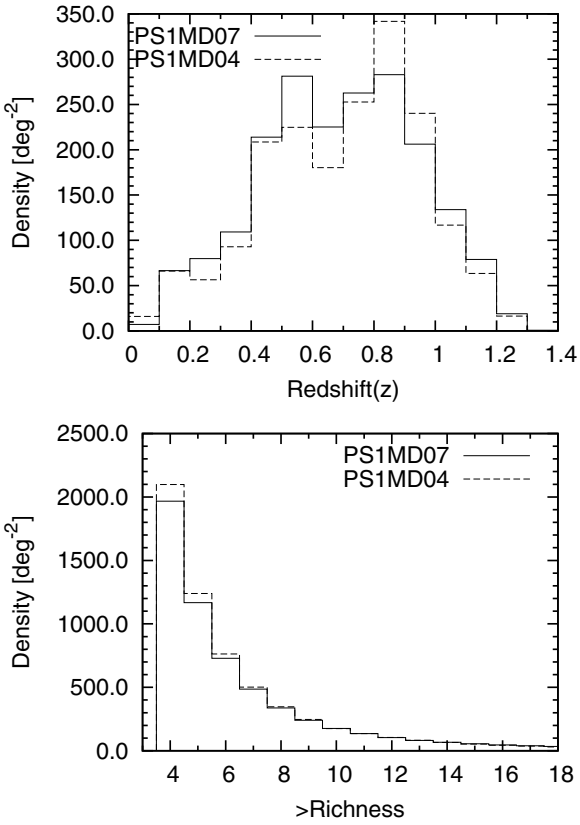

Figure 19. Number density as a function of redshift (top) and threshold richness (bottom) for the PS1MD04 group catalog (the dashed line), using the second optimization strategy, and the PS1MD07 group catalog (the solid line).

z accuracy ~0.03, and the values of $p_1 = 53\%$ and $c_1 = 46\%$ at the minimal $\widetilde{g}_1$ for PS1MD07 catalog with "poorer" photo-z accuracy ~0.054. The optimal performance from these two group catalogs is consistent with that derived from the Durham mock catalog with similar simulated photo-z accuracies.

9. To assess how well PFOF can recover blue and red group galaxies, we make use of group galaxies with spectroscopic redshifts in the EGS and PS1MD07 group catalogs to estimate the recovering rate for red and blue group galaxies. We find that the recovering rate is roughly the same for blue and red group galaxies ~70% in both the EGS and PS1MD07 samples, demonstrating that PFOF detection has no color bias for galaxy groups.
10. To further examine the performance of the PFOF, we match two PFOF group catalogs, COSMOS and PS1MD04, to the *XMM-Newton* plus *Chandra* X-ray catalog to understand how well we may recover X-ray sources. The matched fraction for PFOF COSMOS groups is ~85% with a significance of 5.0, and the matched fraction for PFOF PS1MD04 groups is comparable, ~87% but with a lower significance of 1.5, where the significance is defined as the ratio of the matched fraction from the X-ray catalog to the average fraction from the random catalogs. The matched fractions, 85 and 87%, are close to their respective maximum matched fractions, 89.9 and 91.4%, implying that the subset optimization is successful.

To conclude, we find that the performance of PFOF does not drop significantly with the photo-z accuracy in the range between 0.03 and 0.07 for the mock tests. We also find that the subset optimization is successful for PFOF group finding, and PFOF can be applied to a real sample with PS1-like photo-z accuracy $\sigma_{\Delta z/(1+z_s)} \sim 0.05$ with the purity and completeness reaching ~0.5 from the observational data sets. In addition, we also show that PFOF can detect blue galaxies well and the recovery rate is roughly the same for red (~68.3%) and for blue (~67.3%) group galaxies with spectral-z in the EGS and is ~73.6% for red and ~71.5% in PS1MD07, and thus, demonstrate the capability of PFOF to find blue members in a group or cluster.

The purpose for this paper is to illustrate the capability of PFOF to find groups and clusters with photo-z accuracy achieved by PS1-like surveys, but not to release catalogs at this point. In the near future, we plan to release group catalogs of PS1 MDS by combining grouping results from ORCA (Murphy et al. 2012) and the PFOF algorithms for future science studies. In addition, to make the PFOF group finding applicable, we find that a subset with a high sampling rate of spectral-z catalogs is necessary, and we thus strongly suggest that a photometric survey should be accompanied with a spectral-z survey with a high sampling rate.

We thank R. Bower, M. Takada, and M. Oguri for helpful discussions on our algorithm and PFOF applications, and P. Price for the valuable comments. We also thank Brian F. Gerke for providing us with the DEEP2 group catalogs for the PFOF training. The work is supported in part by the National Science Council of Taiwan under the grants NSC101-2811-M-002-075, NSC99-2112-M-001-003-MY3, NSC101-2112-M-001-011-MY2, and NSC101-2628-M-008-002. This research is Based on zCOSMOS observations carried out using the Very Large Telescope at the ESO Paranal Observatory under Programme ID LP175.A-0839. Funding for the DEEP2 Galaxy Redshift Survey has been provided by NSF grants AST-95-09298, AST-0071048, AST-0507428, and AST-0507483 as well as NASA LTSA grant NNG04GC89G. The Pan-STARRS1 Surveys (PS1) have been made possible through contributions of the Institute for Astronomy, the University of Hawaii, the Pan-STARRS Project Office, the Max-Planck Society and its participating institutes, the Max Planck Institute for Astronomy Heidelberg and the Max Planck Institute for Extraterrestrial Physics Garching, The Johns Hopkins University, Durham University, the University of Edinburgh, Queen's University Belfast, the Harvard-Smithsonian Center for Astrophysics, the Las Cumbres Observatory Global Telescope Network Incorporated, the National Central University of Taiwan, the Space Telescope Science Institute, the National Aeronautics and Space Administration under grant No. NNX08AR22G issued through the Planetary Science Division of the NASA Science Mission Directorate, the National Science Foundation under grant No. AST-1238877, and the University of Maryland, and Eotvos Lorand University (ELTE). PS1 images and catalogs will be made available through a Pan-STARRS PS1 data release by STScI. We close with thanks to the Hawaiian people for the use of their sacred mountain.

REFERENCES

Allen, S. W., Evrard, A. E., & Mantz, A. B. 2011, ARA&A, 49, 409
Bahcall, N. A., McKay, T. A., Annis, J., et al. 2003, ApJS, 148, 243
Bertin, E., & Arnouts, S. 1996, A&AS, 117, 393
Bertin, E., Mellier, Y., Radovich, M., et al. 2002, in ASP Conf. Proc. 281, Astronomical Data Analysis Software and Systems XI, ed. D. A. Bohlender, D. Durand, & T. H. Handley (San Francisco, CA: ASP), 228
Blumenthal, G. R., Faber, S. M., Primack, J. R., & Rees, M. J. 1984, Natur, 311, 517
Borgani, S., Rosati, P., Tozzi, P., et al. 2001, ApJ, 561, 13

Brammer, G. B., van Dokkum, P. G., & Coppi, P. 2008, ApJ, 686, 1503
Carlberg, R. G., Yee, H. K. C., Ellingson, E., et al. 1996, ApJ, 462, 32
Carlstrom, J. E., Holder, G. P., & Reese, E. D. 2002, ARA&A, 40, 643
Chambers, K. 2006, in Proc. Advanced Maui Optical and Space Surveillance Technologies Conference, ed. S. Ryan (Kihei, HI: The Maui Economic Development Board), E39
Chambers, K. C. 2011, BAAS, 43, 222.02
Cole, S., Lacey, C. G., Baugh, C. M., & Frenk, C. S. 2000, MNRAS, 319, 168
Davis, M., Efstathiou, G. S., Frenk, C. S., & White, S. D. M. 1985, ApJ, 292, 371
Davis, M., Faber, S. M., Newman, J., et al. 2003, Proc. SPIE, 4834, 161
Dekel, A., & Birnboim, Y. 2006, MNRAS, 368, 2
de Ravel, Kampczyk, P., Le Fèvre, O., et al. 2011, A&A, submitted (arXiv:1104.5470v1)
Ebeling, H., Edge, A. C., Burgett, W. S., et al. 2013, MNRAS, 432, 62
Eke, V. R., Baugh, C. M., Cole, S., et al. 2004, MNRAS, 348, 866
Faber, S. M., Phillips, A. C., Kibrick, R. I., et al. 2003, Proc. SPIE, 4841, 1657
Frieman, Joshua, & Dark Energy Survey Collaboration 2013, BAAS, 221, 335.01
George, M. R., Leauthaud, A., Bundy, K., et al. 2011, ApJ, 742, 125
Gerke, B. F., Newman, J. A., Davis, M., et al. 2005, ApJ, 625, 6
Gerke, B. F., Newman, J. A., Davis, M., et al. 2012, ApJ, 751, 50
Gilbank, D. G., & Balogh, M. L. 2008, MNRAS, 385, L116
Gillis, B. R., & Hudson, M. J. 2011, MNRAS, 410, 13
Gladders, M. D., & Yee, H. K. C. 2000, AJ, 120, 2148
Guo, Q., White, S., Boylan-Kolchin, M., et al. 2011, MNRAS, 413, 101
Huang, J.-S., Faber, S. M., Willmer, C. N. A., et al. 2013, ApJ, 766, 21
Huchra, J. P., & Geller, M. J. 1982, ApJ, 257, 423
Ilbert, O., Capak, P., Salvato, M., et al. 2009, ApJ, 690, 1236
Ivezic, Z., et al. (LSST Collaboration) 2008, preprint (arXiv:0805.2366)
Jian, H.-Y., Lin, L., Chiueh, T., et al. 2012, ApJ, 754, 26
Kaiser, N., Aussel, H., Burke, B. E., et al. 2002, Proc. SPIE, 4836, 154
Kaiser, N., Burgett, W., Chambers, K., et al. 2010, Proc. SPIE, 7733, 77330E
Kampczyk, P., Lilly, S. J., de Ravel, L., et al. 2013, ApJ, 762, 43
Knobel, C., Lilly, S. J., Iovino, A., et al. 2009, ApJ, 697, 1842
Knobel, C., Lilly, S. J., Iovino, A., et al. 2012, ApJ, 753, 121
Koester, B. P., McKay, T. A., Annis, J., et al. 2007, ApJ, 660, 221
Lagos, C. D. P., Bayet, E., Baugh, C. M., et al. 2012, MNRAS, 426, 2142
Lagos, C. D. P., Lacey, C. G., Baugh, C. M., Bower, R. G., & Benson, A. J. 2011, MNRAS, 416, 1566
Li, I. H., & Yee, H. K. C. 2008, AJ, 135, 809
Lilly, S. J., Le Fèvre, O., Renzini, A., et al. 2007, ApJS, 172, 70
Lin, K.-Y., Woo, T.-P., Tseng, Y.-H., Lin, L., & Chiueh, T. 2004, ApJ, 608, 1
Lin, L., Cooper, M. C., Jian, H.-Y., et al. 2010, ApJ, 718, 1158
Lin, L., Jian, H.-Y., Foucaud, S., et al. 2014, ApJ, 782, 33
Lin, Y.-T., Mohr, J. J., & Stanford, S. A. 2004, ApJ, 610, 745
Liu, H. B., Hsieh, B. C., Ho, Paul T. P., Lin, L., & Yan, R. 2008, ApJ, 681, 1046
Magnier, E. 2006, in Proc. Advanced Maui Optical and Space Surveillance Technologies Conference, ed. S. Ryan (Kihei, HI: The Maui Economic Development Board), E5
Magnier, E. 2007, in ASP Conf. Ser. 364, The Future of Photometric, Spectrophotometric and Polarimetric Standardization, ed. C. Sterken (San Francisco, CA: ASP), 153
Magnier, E. A., Liu, M., Monet, D. G., & Chambers, K. C. 2008, in IAU Symp. 248, A Giant Step: From Milli- to Micro-arcsecond Astrometry, ed. W. J. Jin, I. Platais, & M. A. C. Perryman (Cambridge: Cambridge Univ. Press), 553
Magnier, E. A., Schlafly, E., Finkbeiner, D., et al. 2013, ApJS, 205, 20
Mantz, A., Allen, S. W., Ebeling, H., & Rapetti, D. 2008, MNRAS, 387, 1179
Marinoni, C., Davis, M., Newman, J. A., & Coil, A. L. 2002, ApJ, 580, 122
Merson, A. I., Baugh, C. M., Helly, J. C., et al. 2013, MNRAS, 429, 556
Milkeraitis, M., vanWaerbeke, L., Heymans, C., et al. 2010, MNRAS, 406, 673
Murphy, D. N. A., Geach, J. E., & Bower, R. G. 2012, MNRAS, 420, 1861
Newman, J. A., Cooper, M. C., Davis, M., et al. 2013, ApJS, 208, 5
Oemler, A. 1974, ApJ, 194, 1
Peebles, P. J. E. 1982, ApJL, 263, L1
Postman, M., Lubin, L. M., Gunn, J. E., et al. 1996, AJ, 111, 615
Saglia, R. P., Tonry, J. L., Bender, R., et al. 2012, ApJ, 746, 128
Sarazin, C. L. 1986, RvMP, 58, 1
Schlafly, E. F., Finkbeiner, D. P., Juric, M., et al. 2012, ApJ, 756, 158
Schuecker, P., Böhringer, H., Collins, C. A., & Guzzo, L. 2003, A&A, 398, 867
Scoville, N. Z., Abraham, R. G., Aussel, H., et al. 2007, ApJS, 172, 38
Sheldon, E. S., Johnston, D. E., Frieman, J. A., et al. 2004, AJ, 127, 2544
Smail, I., Swinbank, A. M., Richard, J., et al. 2007, ApJL, 654, L33
Springel, V., White, S. D. M., Jenkins, A., et al. 2005, Natur, 435, 629
Springel, V., White, S. D. M., Tormen, G., & KauRmann, G. 2001, MNRAS, 328, 726
Stubbs, C. W., Doherty, P., Cramer, C., et al. 2010, ApJS, 191, 376
Sunyaev, R. A., & Zel'dovich, I. B. 1980, ARA&A, 18, 537
Takada, M. 2010, in AIP Conf. Proc. 1279, Deciphering the Ancient Universe with Gamma-Ray Bursts, ed. N. Kawai & S. Nagataki (Melville, NY: AIP), 120
Tonry, J. L., Stubbs, C. W., Lykke, K. R., et al. 2012, ApJ, 750, 99
Voit, G. M. 2005, RvMP, 77, 207
Wen, Z. L., Han, J. L., & Liu, F. S. 2009, ApJS, 183, 197
Wittman, D., Dell'Antonio, I. P., Hughes, J. P., et al. 2006, ApJ, 643, 128
Yang, X., Mo, H. J., van den Bosch, F. C., & Jing, Y. P. 2005, MNRAS, 356, 1293